TU WIEN
DEPARTMENT OF GEODESY
AND GEOINFORMATION

DIPLOMARBEIT

Position change of the northernmost VLBI telescopes in Ny-Alesund, Svalbard

zur Erlangung des akademischen Grades

Diplom-Ingenieur

ausgeführt am Department für
Geodäsie und Geoinformation
Forschungsbereich Höhere Geodäsie
der Technischen Universität Wien

unter Anleitung von
Ass. Prof. Dr.in. Hana Krasna
und
Prof. Dr. Johannes Böhm

Durch

Gentrit Krasniqi, Bsc

Matrikelnummer: 11732281

Wien, 23.2.2024 _____ _____

Unterschrift (Verfasser/in) Unterschrift (Betreuer/in)

Eidesstaatliche Erklärung

Ich erkläre an Eides statt, dass die vorliegende Arbeit nach den anerkannten Grundsätzen für wissenschaftliche Abhandlungen von mir selbstständig erstellt wurde. Alle verwendeten Hilfsmittel, insbesondere die zugrunde gelegte Literatur, sind in dieser Arbeit genannt und aufgelistet. Die aus den Quellen wörtlich entnommenen Stellen, sind als solche kenntlich gemacht.

Das Thema dieser Arbeit wurde von mir bisher weder im In- noch Ausland einer Beurteilerin/ einem Beurteiler zur Begutachtung in irgendeiner Form als Prüfungsarbeit vorgelegt. Diese Arbeit stimmt mit der von den Begutachterinnen/Begutachtern beurteilten Arbeit überein.

Wien, 23.02.2024 Gentrit Krasniqi

Acknowledgements

First and foremost, I paise and thank God, who has granted us countless blessings.

My warm gratitude extends to my family for their constant support, love, and belief in my abilities.

Additionally, I would also like to extend my appreciation to my advisors Prof. Dr. Hana Krasna and Prof. Dr. Johannes Böhm for their invaluable guidance. Without their guidance, this work would not be possible.

Lastly, I am thankful to all my relatives, friends, and colleagues who supported and advised me during my master's studies.

Dedication

To my grandfather B.K.

and parents,

M&M.

Abstract

Very Long Baseline Interferometry (VLBI) is a space geometric observing technique, the goal of which is to monitor the kinematics of interest points on Earth and in space. The observing instruments of VLBI are approximately 40 radio telescopes distributed throughout the world that simultaneously receive electromagnetic radiation emitted by compact objects in space, such as quasars. This technique has applications in geodesy, astrometry and astronomy (Nothnagel et.al., 2023).

This master thesis aimed to analyze time series data from two of the northernmost VLBI telescopes, namely Nyales20 and Nyale13s, which are located in Svalbard, Norway. The thesis provided position time series data for both stations, which helped us to understand their position over the study period; to determine whether they exhibit discrepancies, especially in height biases; and finally, to analyze whether these changes could be related to factors such as glacier melting.

Furthermore, this thesis evaluated the availability of sufficient parallel sessions for transferring velocity information from the legacy system (Nyales20) to the VGOS new generation (Nyale13s); then, it analyzed whether extending the working time of the legacy telescope Nyales20 is beneficial even though its working timespan has surpassed 30 years. Finally, this thesis compared the observed uplift trends from the VLBI and GNSS time series.

The analysis was conducted using the Vienna VLBI Software (VieVS), which is a VLBI analysis software for geodesy and astrometry. Additionally, Vienna Scheduling software (VieSched++), which is part of VieVS, was used to generate and simulate IVS-R1 and IVS-R4 schedules, to address the objective of this study concerning the prolongation consideration of the legacy telescope Nyales20.

The real data sets were directly downloaded in open-source vgosDB format, which is the IVS standard format for storing, transmitting, and archiving VLBI data (Webiste: NASA Earth Data).

The results revealed height biases in the VLBI and GNSS time series data with respect to a priori catalog positions. This supported geophysical processes (e.g., glacier melting) as potential contributing factors.

Furthermore, based on the velocities obtained for both stations, while also considering the number of parallel sessions (77 sessions), we were able to confirm that the transfer of velocities from the legacy telescope Nyales20 to the VGOS telescope Nyale13s can be achieved.

Finally, addressing the impact of the Nyales20 telescope, our analysis revealed that excluding Nyales20 telescope led to an increase in mean formal error and repeatability values of several percent for Earth orientation parameters. This suggests that maintaining both telescopes within the network enhances accuracy. However, economic concerns and safety reasons influenced the decision to dismantle Nyales20 on August 14, 2023 (Garcia-Espada et.al., 2022). Despite its positive impact on quality of the data, the practical implications encourage its cancellation.

Kurzfassung

Die Very Long Baseline Interferometry (VLBI) ist ein geometrisches Beobachtungsverfahren, deren Ziel es ist, die Kinematik von ausgewählten Punkten auf der Erde und im Weltraum zu beobachten. Die Beobachtungsinstrumente der VLBI sind rund 40 Radioteleskope, weltweit verteilt, die gleichzeitig elektromagnetische Strahlung von kompakten Objekten im Weltraum, wie Quasaren, empfangen. Diese Technik findet Anwendung in der Geodäsie, Astrometrie und Astronomie (Nothnagel et. al. , 2023).

Ziel der Masterarbeit war es, Zeitreihendaten von zwei der nördlichsten VLBI-Teleskope, nämlich Nyales20 und Nyale13s, zu analysieren. Diese Masterarbeit behandelt Positions-Zeitreihendaten für beide Stationen, mit denen ihre Position während des Untersuchungszeitraums beobachtet wurde. Ziel war es festzustellen, ob die Positionen der Stationen Diskrepanzen aufweisen, insbesondere Höhenverzerrungen, und abschließend zu analysieren, ob diese Veränderungen mit Faktoren wie der Gletscherschmelze zusammenhängen könnten.

Darüber hinaus wurde in dieser Arbeit die Verfügbarkeit ausreichender paralleler Sessions für die Übertragung von Geschwindigkeitsinformationen vom Altsystem (Nyales20) auf das VGOS der neuen Generation (Nyale13s) bewertet. Anschließend wurde analysiert, ob eine Verlängerung der Betriebszeit des Altteleskops Nyales20 sinnvoll ist, obwohl seine geplante Betriebszeit von 30 Jahren überschritten wurde. Abschließend wurden in dieser Arbeit die beobachteten Positionsänderungen in Lage und Höhe aus den VLBI- und GNSS-Zeitreihen verglichen. Die Analyse wurde mit der Vienna VLBI Software (VieVS) durchgeführt, einer VLBI-Analyse-Software für Geodäsie und Astrometrie. Zusätzlich wurde die Vienna Scheduling Software (VieSched++), die Teil von VieVS ist, zur Generierung und Simulation von IVS-R1- und IVS-R4-schedules eingesetzt, um das Ziel der vorliegenden Studie bezüglich der Verlängerungsbetrachtung des alten Teleskops Nyales20 zu erreichen.

Die Datensätze wurden im Open-Source-Format vgosDB heruntergeladen, dem IVS-Standardformat zur Speicherung, Übertragung und Archivierung von VLBI-Daten (NASA Earth Data). Die Ergebnisse zeigen Höhenunterschiede zwischen den VLBI- und GNSS-Zeitreihen in Bezug auf die a priori Katalogpositionen. Dies spricht für geophysikalische Prozesse (z. B. Gletscherschmelze) als mögliche Einflussfaktoren. Darüber hinaus konnte anhand der für beide Stationen ermittelten Geschwindigkeiten und unter Berücksichtigung der Anzahl der parallelen Sessions (77 Sessions) bestätigt werden, dass die Übertragung der Geschwindigkeiten vom Altteleskop Nyales20 auf das VGOS-Teleskop Nyale13s möglich ist.

Abschließend wurde festgestellt, dass der Ausschluss des Altteleskop Nyales20 zu einem Anstieg der mittleren formalen Fehler- und Wiederholbarkeitswerte der Erdorientierungsparameter um einige Prozent führte.

Dies deutet darauf hin, dass die Beibehaltung beider Teleskope im Netzwerk die Genauigkeit erhöht. Dennoch führten Wirtschafts- und Sicherheitsbedenken zur Entscheidung, Nyales20 am 14. August 2023 abzubauen (Garcia-Espada et al., 2022). Trotz der positiven Auswirkungen auf die Qualität der Daten sprachen die praktischen Erwägungen für eine Schließung.

Table of Contents

List of Figures

List of Tables

List of Abbreviations

VLBI *Very Long Baseline Interferometry*

GNSS *Global Navigation Satellite Systems*

DORIS *Doppler Orbitography and Radiopositioning Integrated by Satellites*

SLR *Satellite Laser Ranging*

LLR *Lunar Laser Raning*

ITRF *International Terrestrial Reference Frame*

ITRS *International Terrestrial Reference System*

ICRF *International Celestial Reference Frame*

ICRS *International Celestial Reference System*

EOP *Earth Orientation Parameters*

GCRS *Geocentric Celestial Reference System*

IVS *International VLBI Service for Geodesy and Astrometry*

VGOS *VLBI Global Observing System (New Generation)*

USNO *U.S. Naval Observatory*

NASA *National Aeronautics and Space Administration*

NRAO *National Radio Astronomy Observatory*

VLBI2010 *Legacy VLBI System*

CIP *Celestial Intermediate Pole*

dUT1 *deviation of Universal Time 1 from Uniform Atomic Time*

UT1 *Universal Time 1*

UTC *Universal Time Coordinated (Uniform Atomic Time)*

VieVS *Vienna VLBI Software*

VieSched++ *Vienna Scheduling Software*

NY *Nyales20*

Ns *Nyale13s (Ny-Alesund South antenna)*

Nn *Nyale13n (Ny-Alesund North antenna)*

NMA *The Norwegian Mapping Authority*

GBO *Green Bank Observatory*

MJD Modified Julian Date

IERS International Earth Rotation and Reference Systems Service

NNR No-Net-Rotation

NNT No-Net-Translation

1. Introduction

1.1. Space Geodetic Techniques

Space geodetic techniques are crucial tools in the field of geodesy and astrometry. They provide critical information for the positioning, navigation, and monitoring of dynamic Earth processes, such as plate tectonics, polar ice cap melting, sea level rise, and atmospheric phenomena.

The term “space geodesy” refers to the use of space-based objects, such as artificial satellites, moon or instruments on the moon (reflectors), other planets in the solar system, optically visible stars, and distant cosmic radio sources (billions of light years away; Nothnagel et.al., 2023).

A variety of space-geodetic techniques exist, such as Very Long Baseline Interferometry (VLBI), Doppler Orbitography and Radiopositioning Integrated by Satellites (DORIS), Lunar Laser Ranging (LLR), Satellite Laser Ranging (SLR), and the Global Navigation Satellite Service (GNSS).

Among these techniques, VLBI stands out as a microwave-based method with diverse applications in astronomy, geodesy, astrometry, and astronomy (Nothnagel, et.al, 2023).

“Regarding geodesy and astrometry, VLBI plays an essential role in the realization and maintenance of the International Celestial Reference Frames (ICRF) and contributes significantly to the International Terrestrial Reference Frame (ITRF), especially for its scale. Furthermore, it is also the only technique that provides the full set of Earth orientation parameters (EOPs) specifically polar motion, nutation, and precession. Hence, VLBI plays an essential role in positioning and navigation on Earth and in Space” (Schuh & Böhm, 2012).

1.2. Aims of the study

The goal of this study was to analyze time series data from two of the northernmost VLBI telescopes, namely Nyales20 and Nyale13s.

This study aimed to address the following objectives:

- To generate and examine position time series data for both VLBI stations (Ny, Ns) and GNSS site (NYA2), to understand their respective positions over time;
- To compare the position changes observed in both VLBI antennas to determine whether they agree or exhibit any significant discrepancies, especially changes in the height component;
- To compare the observed uplift trends from the VLBI time series data with the GNSS time series;
- To evaluate the availability of sufficient parallel sessions for transferring velocity information from the legacy system (Nyales20) to the new generation VLBI Global Observing System (Nyale13s);
- To analyze whether it is necessary or beneficial to extend the working time of the legacy telescope Nyales20 to improve data quality.

Overall, this study aims to gain insights into position changes, velocities, and factors influencing the changes between VLBI-telescopes Nyales20, Nyale13s and GNSS station NYA2. Additionally, to

evaluate whether transferring velocities information from Nyales20 to Nyale13s is possible after 3 years mixed-mode operation. Finally, to determine whether extending the working time of Nyales20 is reasonable.

1.3. Thesis outline

This master's thesis consists of seven chapters, as follows:

- **Chapter 1:** provides general information about VLBI and our study objectives;
- **Chapter 2:** begins with an overview of VLBI's history and its measurement principle. It then elaborates on its applications and products, namely reference frames and EOPs. Finally, it discusses current and future VLBI systems;
- **Chater 3**: provides general information about the Ny-Alesund Observatory, followed by details about its legacy (Nyales20) and VGOS twin (Nyale13s and Nyale13n) telescopes;
- **Chapter 4:** outlines the data used for our analysis. Additionally, it describes the concept of VieVS and its workflow for this case study. Lastly, it provides an explanation about VieSched++;
- **Chapter 5:** gives a detailed explanation of the parameter estimation process employed for this study case, namely Gauss-Markov Model.
- **Chapter 6**: present the results of our comprehensive. It provides an understanding of their position time series, changes in position, and their behavior in the context of glacier melting, and to evaluate their suitability for further scientific investigations;
- **Chapter 7**: the main points of this study are discussed.

2. General

This chapter begins with a brief overview of VLBI's history and its measurement principle. It then elaborates on its applications and products, namely reference frames and EOPs. Finally, it discusses current and future VLBI systems.

2.1. Early years of VLBI

The first attempt to investigate sources of radio noise that could distribute transatlantic communication was made in 1928 by Jansky, who discovered the first extra-terrestrial radio source, now known to be the center of our galaxy the Milky Way, which is called Sagittarius A (Sgr A*).

In the 1950s, VLBI was a product of radio interferometry with cable-connected elements, which meant that the observations could not be spaced far apart from each other; thus, measurements of very large baselines were impossible (Cohen et al. 1968). This limited the potential resolution of the technique, as finer details in celestial objects require longer baselines. Later in the 1960s, advances in technology allowed for the development of high-speed tape recorders and atomic frequency and time standards (Guochang Xu, 2013). These technologies allowed for phase-coherent Michelson-type interferometers with no physical connection between the elements, enabling measurements of very large baselines (Guochang Xu, 2013). This eliminated the need for cable connections, allowing telescopes to be placed anywhere in the world, hence also making it possible to measure the transatlantic baseline (Schuh & Böhm et.al 2013)

The first experiments were conducted by the Haystack/MIT group on the Haystack to Green Bank baseline. These experiments demonstrated the potential of VLBI for measuring the rotation of the Earth as well as for studying atmospheric effects and the Earth's gravitational field (Hinteregger et al. 1972).

"In 1967, three groups one Canadian team, a collaboration between the National Radio Astronomy Observatory (NRAO) and Cornell University, and the MIT and Haystack Observatory worked independently to achieve the first VLBI observation. At the same time a Russian group was also working on the development of VLBI" (Schuh & Böhm et.al 2013).

The development and successful operation of two-station interferometers by the three independent groups led to the first VLBI observation in 1967.

The first geodetic observation used MKI system, which could record only 0.72 Mbit/sec (Whitney et al. 1967), whereas modern systems can record at 1024 Mbit/sec or even more, such as new-generation VGOS, which can record up to Gbits/sec. The invention of the bandwidth synthesis technique was the key point that helped scientists to overcome tape-recording-limitations in terms of recordable bandwidth and improve station position precision.

The baseline between the Haystack Observatory in Northern Massachusetts and the NRAO of Green Bank, West Virginia, USA (approximately 845km) was the first experiment and longest distance aimed at achieving geodetic accuracy using the VLBI measurement principle. Since then, the precision of station position has improved dramatically, from a few meters to the current level of 1 cm accuracy or even better (Schuh & Böhm et.al 2013).

The main factors that helped to improve precision were equipment improvements, such as wider recording bandwidths, dual frequency observation, lower system temperature, and phase calibration.

The developments in geometric techniques are listed in Table 2.1:

Technique	Accuracy
1960 (Stellar triangulation)	Approx. 100m
1970 SLR first generation	Approx. 10m
1970 Transit (Doppler)	0.3m … 1m
1980 SLR third Generation	3cm … 10cm
1980 VLBI (Mark III)	3cm … 10cm
1990 VLBI/SLR/GNSS developments	1cm
2000 Combination of space geo techniques	3mm
VGOS Goal	1mm and 0.1 mm/year

Table 2.1. The development of space-geodetic techniques (Böhm, 2021).

2.2. Measurement principle of VLBI

VLBI is a space geometric observing technique in which the observing instruments are radio telescopes that receive the electromagnetic radiation emitted by distant objects in space (a few billions light years away), such as quasars. There are two different types of radio telescopes: 20-m telescopes, which represent the legacy system and the 13-m telescopes, which represent the new-generation, VGOS system (Nothnagel et.al., 2023).

There are more than 40 active VLBI radio telescopes, and they are distributed throughout various countries to maintain overall coverage. They simultaneously observe extragalactic radio sources known as “quasars”. Quasars and other extra-galactic radio sources are the primary objects observed in VLBI (Nothnagel et.al., 2023).

Since radiation is emitted by sources billions of light years away, the signals arrive on Earth as a random noise with mostly a plane wavefront in the frequency band (Nothnagel et.al., 2023).

The VLBI observable is a travel time, which represents the difference between the arrival time of the radiation at two different telescopes (Delva et al. 2023).

Figure 2.1 illustrates the geometric principle, where the positions (1 & 2) indicate the VLBI observatories, specifically radio telescopes; s(t) is the observed source, and b is the baseline vector (Schuh & Böhm, 2013):

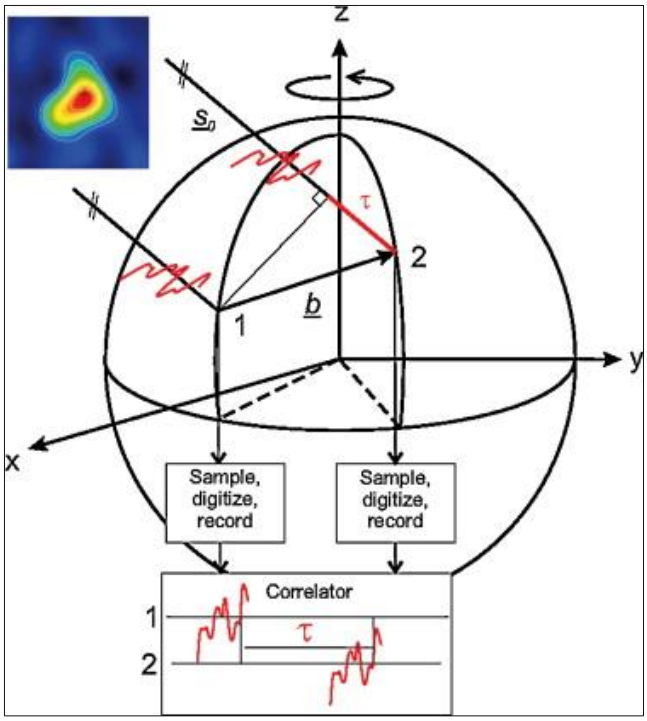

Figure 2.1 Measurement principle of VLBI (Schuh & Böhm, 2013).

Radiation emitted from a single source (point) but received by the two telescopes is considered to have two noise patterns (Nothnagel et.al., 2023). It arrives on Earth at different times, denoted t1 and t2, due to Earth's rotation.

By measuring the time delays between the signals received at different telescopes, VLBI can determine the following: (a) telescope coordinates, (b) the (angular) parameters of the Earth's variable rotation (c) the angular positions of galactic and extra galactic radio sources (Nothnagel et.al., 2023).

According to Schuh und Behrend (2012) "Tau" (τ) can be calculated using a scalar product of the baseline (b) and observed source (s) divided by the velocity of light (c)", as in Equation (1.1):

$$\tau = \frac{-b' * s}{c} = (t_2 - t_1) \qquad (2.1)$$

Since the end of the 1970s, the VLBI geodetic observations have been performed in two different frequency bands, namely the S-band (2.3 GHz) and the X-band (8.4 GHz). By contrast, the new-generation VGOS performs observations in a frequency band between 2 and 14 GHz (Schuh & Böhm et.al 2013).

Radio telescopes observe the quasar (s(t)) simultaneously, and each station saves the observed radio signal in S/X frequency bands with time stamps using highly stable and precise atomic clocks known as hydrogen masers "H-maser". To obtain the group delays, recorded and time-tagged data are sent to a correlator center, where the correlation between signals is determined. These group delays, or differences in signal's arrival times are used for geodetic and astrometric applications (Schuh & Böhm, 2013).

For a further explanation, see the wotk of: Schuh and Böhm (2013).

2.3. Applications and products

IVS stands for International VLBI Service for Geodesy and Astrometry. It was founded in 1999, by corporation of international VLBI organisations, whose goal is to coordinate the global components on an international level (IVS Website: https://ivscc.gsfc.nasa.gov).

The IVS plays a crucial role in providing data and products for the scientific community. It contributes ICRF by determining the positions of extragalactic radio sources. The IVS also contributes to the TRF by providing the positions and velocities of radio telescopes. Additionally, it offers a time series of EOPs, which are derived from 24-hour sessions and daily 1-hour intensive sessions (IVS Website).

In recent years, the IVS has been particularly focused on the development of the VGOS (see chapters 2.4 and 3). “This system utilizes broadband delay, which involves the use of four or more frequency bands ranging from 2.5 to 14 GHz. Observations are made using fast-slewing, 12-meter-class antennas at a high data rate of 8 Gbps and above. The increased sampling of the sky, compared with the legacy system, allows for a reduction in error components. This, along with a reduction in systematic errors, is expected to result in an overall accuracy of 1 mm.” (Schuh and Behrend, 2012).

Figure 2.2 presents the VGOS network:

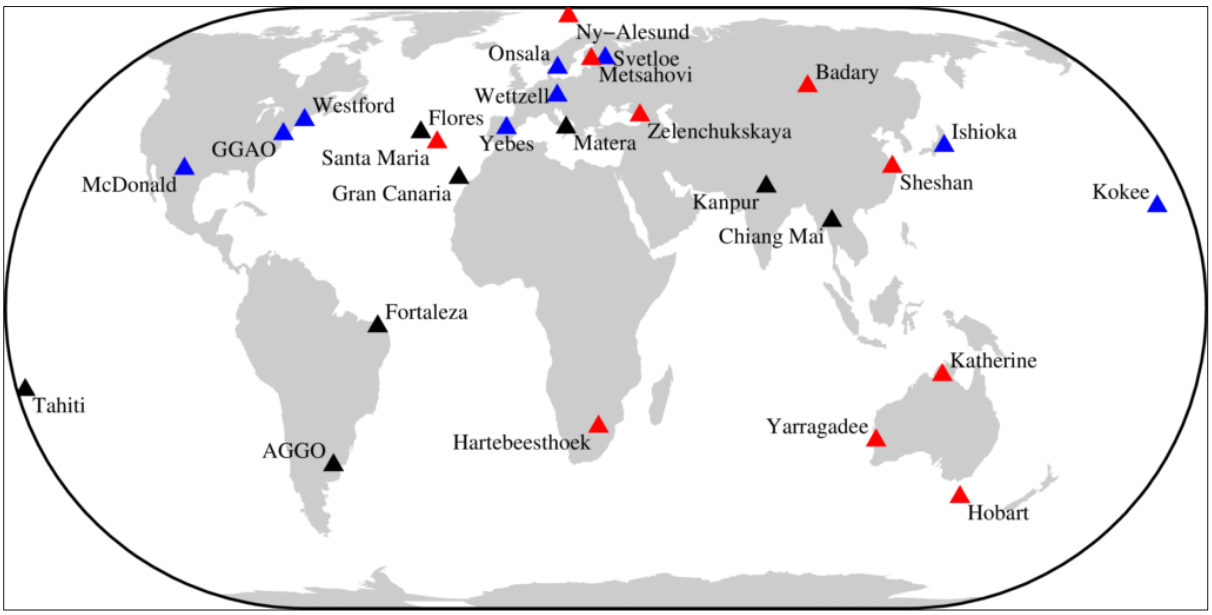

Figure 2.2. The VGOS network (*International VLBI Service for Geodesy and Astrometry | GGOS*).

For more detailed information, visit the IVS website at **https://ivscc.gsfc.nasa.gov/.**

In the following sections, brief description of main IVS products is provided, specifically reference frames and EOPs.

2.3.1. Reference Frames

Before we closely elaborate on the reference frames, it is crucial to distinguish between reference frames and reference systems.

A reference system covers the establishment of a coordinate system, including aspects such as its origin and, orientation, as well as the fundamental physical models that support it. By contrast, a reference frame represents the practical implementation of a reference system through observations (B*öhm, 2021*).

Reference frames, a crucial development in geodesy, describe the movements of objects. To further elaborate, introductory math courses, typically begin by depicting a coordinate system with an origin at the intersection of axes, before determining point locations by measuring distances along the axes from this origin to ascertain their respective coordinate components. However, in space geodesy, localizing the origin or determining the axis direction beforehand is unrealistic. Hence, by convention, coordinates are assigned to points and the origin and axis directions are indirectly derived. This selection is made to maintain the internal configuration, ensuring the relative relationships between points remain undeformed (Nothnagel et.al., 2023).

Reference frames can be further categorized into types, such as the following:

- Celestial reference frames;
- Terrestrial reference frames;
- Height reference frames;
- Gravity reference frames.

In the same concept and stability criteria apply, with the only distinction w.r.t. the TRF that the origin of the CRF is defined a priori by the barycenter, center mass, of the solar system (Nothnagel et.al. 2023).

“The VLBI technique plays a unique role in establishing and maintaining the ICRF, as it is the only space-geodetic technique to contribute to the ICRF’s realization” (Schuh & Böhm, 2013). By contrast, the determination and maintenance of the ITRF is a combination of multiple space-geodetic techniques such as SLR, DORIS, and GNSS” (B*öhm, 2021*).

The following subsections elaborate on the ICRF and ITRF.

2.3.1.1. International Celestial Reference Frames

The ICRF is related to the positions of compact extragalactic radio nuclei, such as quasars, defined by their angular right ascension (α) and declination (δ) angles of an equatorial polar coordinate system (Nothnagel et.al. 2023).

The ICRF defines a barycentric coordinate system, essentially a quasi-inertial system, with its origin located at the barycenter of the solar system (Nothnagel et. Al., 2023).

“Its pole is in the direction defined by the conventional International Astronomical Union (IAU) models for precession (Lieske et al., 1977) and nutation (Seidelmann, 1982). Its origin of right ascensions was implicitly defined by fixing the right ascension of 3C 273B to the Hazard et al. (1971) FK5 value transferred at J2000.0. See Arias et al. (1995)” (IERS website: https://www.iers.org).

Figure 2.3 shows the definition of ICRF:

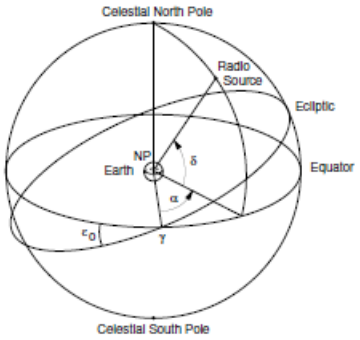

*Figure 2.3. International Celestial Reference Frame (*Nothnagel et.al. 2023).

The ICRF’s importance spans various domains, notably in determining Earth’s orientation in space, which includes phenomena such as nutation and, precession, as well as time measurement. Additionally, it plays a vital role in interplanetary navigation, extragalactic kinematics, satellite orbit calculations, and more.

VLBI stands out as the sole technique capable of observing sources billions of light years away; thus, it is integral to the realization of the ICRF.

The key characteristic of the ICRF is its reliance on celestial sources situated at infinite distances, which serve as ideal directional references. However, due to their weak signal, it is necessary to use large telescopes ranging from 10 to 100 meters and also to allocate extensive (B*öhm, 2021*). These celestial sources, commonly referred to as quasars, emit radiation from active galactic nuclei, which is attributed to mass accretion by supermassive black holes.

The IAU holds authority over the ICRF and has accepted several fundamental CRFs:

- ICRF1, accepted as a fundamental CRF on January 1, 1998;
- ICRF2, accepted as a fundamental CRF on January 1, 2010;
- ICRF3, accepted as a fundamental CRF on January 1, 2019.

ICRF3, the current realization, is determined through VLBI and contains over 4600 sources; specifically, it contains 4536 sources in the S/X Band (2.3 and 8.4 GHz); 824 sources in the K Band (24 GHz); and 678 sources in the X/Ka Band 8.4 and 32 GHz; (B*öhm, 2021*). The axis definition is accurate to 10–20 *μ*as and the position uncertainties have a median error of 0.15 mas, compared with 0.5 mas in ICRF2 (Nothnagel et.al. 2023).

2.3.1.2. International Terrestrial Reference Frame

The ITRF serves a variety of purposes, including determining Earth's figure and orientation and referencing processes occurring at or near its surface such as plate tectonics, earthquakes, and sea level rise. Furthermore, it is crucial for determining satellite orbits and facilitating precise positioning and navigation (B*öhm, 2021*).

The ITRF's establishment involves the collaboration of approximately 40 globally distributed VLBI radio telescopes, through various space-geodetic methods, such as GNSS, VLBI, SLR, and DORIS.

The realization of the ITRF lies in the center of Earth's mass, including its oceans and atmosphere, with measurements in meters (SI) and an orientation based on No-Net-Rotation (NNR) criteria w.r.t. BIH (Bureau International de l'Heure) 1984.

Figure 2.4 presents the definition of ITRF:

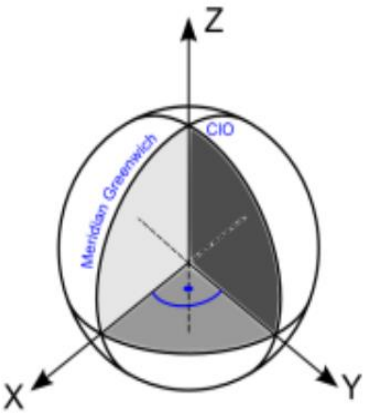

"Original concept for orientation (Cartesian coordinates and velocities):

- z-axis: mean Earth rotation axis of years 1900-1905;
- x-and y-axes in the equatorial plane;
- x-axis intersects Greenwich meridian." (website: *https://transformator.bev.gv.at).*

Figure 2.4. The International Terrestrial Reference Frame (BEV Transformator Web https://transformator.bev.gv.at/).

The first combined conventional global TRF can be considered the BIH Terrestrial System 1984 (BTS84) of the Bureau International de l'Heure (BIH). BTS84 incorporated 14 VLBI telescopes, two LLR telescopes, and 27 SLR telescopes (B*öhm, 2021*).

Over the years, multiple versions of the ITRF have been developed, denoted by years, such as ITRF88, ITRF97, ITRF2000, ITRF2005, ITRF2008, ITRF2014, and ITRF2020.

"In comparison with the previous realizations, which provide station positions, velocities and EOPs, ITRF2020 additionally provides Post-Seismic Deformation (PSD) parametric models for stations subject to major earthquakes, annual and semi-annual periodic terms expressed in the Center of Mass (CM- as sensed by SLR) frame, as well as in the Center of Figure (CF) frame" (ITRF website: https://itrf.ign.fr/).

Following equations (2.2) shows, how the 3D coordinates of a station can be calculated:

$$X(t) = X(t_0) + \dot{X}(t - t_0) + \delta X_{PSD}(t) + \delta X_f(t) \qquad \dots (2.2)$$

Where:

$X(t_0)$ *- station coordinates,* t_0 *– indicating the reference epoch of ITRF2020 (January 1, 2015);*

$X(t - t_0)$ *- velocities;*

$\delta X_{PSD}(t)$ *– position of the station affected by post-seismic deformation (earthquakes);*

$\delta X_f(t)$ *– annual and semi-annual signals (seasonal signals).*

This realization combines the results of the VLBI, SLR, GNSS, and DORIS observing techniques. This combined framework leverages the strengths of each individual method. For instance, VLBI and SLR define the scale of the frame and mutually regulate each other. Moreover, SLR and VLBI determine the frame's origin. Furthermore, the geocenter is one of the crucial products of SLR. The orientation is based on NNR criteria concerning ITRF 2005, utilizing GNSS stations (Nothnagel et.al. 2023).

The following subsections elaborate on EOPs.

2.3.2. Earth orientation parameters

Earth's rotation is not homogenous but is rather affected by spatio-temporal variations, such as internal and external torques. "External torques are produced by the gravitational attractions of the sun, moon and planets, whereas internal torques can be assigned to large-scale geodynamical processes that simulate the exchange of angular momentum between the solid parts of the Earth and the fluid layers (e.g., the atmosphere and, oceans)" (Böhm & Schuh, 2013).

As mentioned earlier, geodetic VLBI is the only space-geodetic technique that helps us to better understand the effects of these spatio-temporal variations on Earth's rotation by providing the complete set of EOPs.

In general, there are five key EOPs, which are described as follows:

- Polar motion (XPO, YPO): This describes the Earth's rotation axis position with respect to the TRF.
- Nutation and precession (NUTX, NUTY): These describe the Earth's rotation axis in space, providing information for understanding its orbital dynamics.
- dUT1 = UT1 – UTC: This refers to the deviation of UT1 (Universal time 1) from the uniform atomic time UTC (Universal Time Coordinated; Nothnagel et.al. 2023).

Figure 2.5 displays the Earth Orientation Parameters:

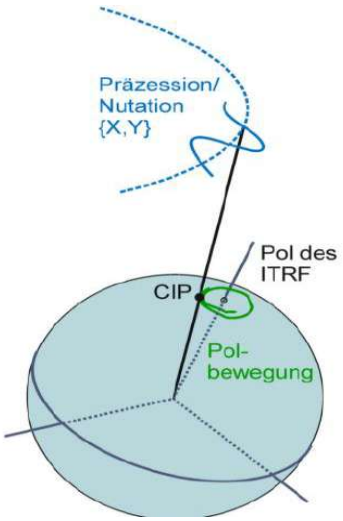

Figure 2.5. Earth orientation parameters (B*öhm, 2021*).

These five parameters are crucial for accurate positioning and navigation both on Earth and in space.

The transition from a barycentric (celestial) system to a terrestrial system is also facilitated through EOPs (Schuh & Behrend, 2012).

The transformation matrix is as follows: **[GCRS] = Q*(t)* · R*(t)* ·W*(t)* · [TRS]** (2.4)

where :

GCRS *Geocentric Celestial Reference System;*

W(t) *polar motion of the celestial intermediate pole w.r.t. the TRF;*

R(t) *Earth's rotation around the celestial intermediate pole;*

Q(t) *precession and nutation (motion of celestial intermediate pole in the CRF);*

TRS *terrestrial reference frame.*

A practical example of the determination of polar motion through the application of the VLBI technique is presented in Figure 2.6:

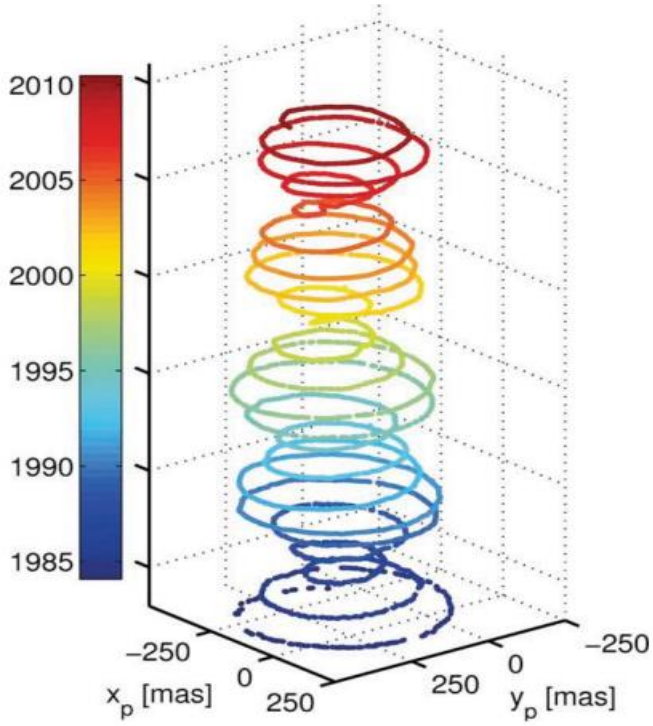

Figure 2.6. Polar motion estimates between 1984 and 2010 through application of VLBI (Schuh & Behrend, 2012).

In the following sections, brief description of current and future VLBI system is provided.

2.4 Current and future VLBI systems

The VGOS represents the latest advancements in modern geodetic VLBI observation concepts, surpassing the legacy S/X band observation systems with its innovative features.

The project itself originated in 2003 with the establishment of the IVS Working Group 3, also known as the “IVS Working Group on VLBI2010” (Nothnagel et al. 2023). Its primary goal was to investigate options for modernising the VLBI system and produce a report.

The report outlined recommendations for a new-generation system that meets specific criteria, including the highest-precision geodetic and astronomic results, low construction and operation costs, and a rapid turnaround of final results.

The IVS Directing Board approved the final report, titled “A Vision for Geodetic VLBI-VLBI2010: Current and Future Requirements for Geodetic VLBI Systems”, in September 2005 (Niell et.al., 2018).

On March 9, 2012, the IVS Directing Board changed the project’s name from VLBI2010 to VGOS to align with the Global Geodetic Observing System (GGOS) of the International Association of Geodesy (IAG) (Nothnagel et al. 2023). This adjustment was prompted by GGOS’s demand for 1mm coordinate and 0.1mm/year velocity accuracy targets on a global scale. Furthermore, continuous measurements for time series of station positions and EOP are completed less than 24 hours after observation (Schuh & Boehm, 2013).

Subsequently, numerous telescopes were constructed and correlation capacity and post-processing software were developed.

In the VLBI2010 project, atmospheric refractive behavior (troposphere) has been the key barrier for the S/X band system. Attaining mm-level accuracy in path length determination was vital for improved geodetic and astrometric outcomes. Employing small (12-m diameter) antennas shortened observation intervals, enabling denser atmospheric sampling. This method improved the estimation of zenith wet delays (ZWDs) with higher precision (Nothnagel et al. 2023).

According to Nothnagel (2023) the signal chain of the VGOS was redesigned for the desired precision, resulting in a four-band system spanning 2 - 14 GHz. A 2GHz lower-limit maintained compatibility with existing S/X band systems, and the broader frequency range maximized the spanned bandwidth effect.

Important to mention is the mixed-mode operation between legacy S/X band radio telescopes and VGOS infrastructure. They will co-exist for some time to link reference frames, both terrestrial and celestial. The so-called mixed-mode sessions are highly valued by the community, as they allow seamless operations of both telescope types (Nothnagel et al. 2023).

More details are provided in Chapter 3.

3. NY-ALESUND Geodetic Earth Observatory

This chapter provides general information about the Ny-Alesund Observatory, followed by details about its legacy (Nyales20) and VGOS twin (Nyale13s and Nyale13n) telescopes.

3.1. Description of Nyales20 and Nyale13s

The Ny-Alesund Observatory is located on the island of Spitsbergen, Norway. It is home to several world-class telescopes, including the legacy telescope Nyales20 (Ny) and the VGOS twin telescope, specifically the Ny-Alesund North antenna (Nn) and South antenna (Ns).

The legacy 20-m radio telescope Ny-Alesund (Ny) was first established at Hamnerabben in Ny-Alesund, Svalbard, in 1993, located at 78.9◦ N 11.9◦, on the west side of Spitsbergen, and is managed by the Norwegian Mapping Authority (NMA). The construction of the telescope started in 1993, and it began operation on October 4, 1994. Since then, it has contributed significantly to the global VLBI regularly participating in the global VLBI S/X sessions and thus contributing to the estimation of CRF, TRF, EOPs.

The 20-m radio telescope was intended for geodetic use and received data in legacy S and X band (Kupiszewski et al. 2020).

Table 3.1 provides general information about Nyales20:

	NY Telescope
geographic longitude:	11° 52′ 11″
geographic latitude:	78° 55′ 45″
diameter telescope:	20m
minimum elevation:	2°

Table 3.1. Basic information about Nyales20 radio telescope (see website: CRAF-Committee on Radio Astronomy Frequencies).

Figure 3.1 displays the VLBI network:

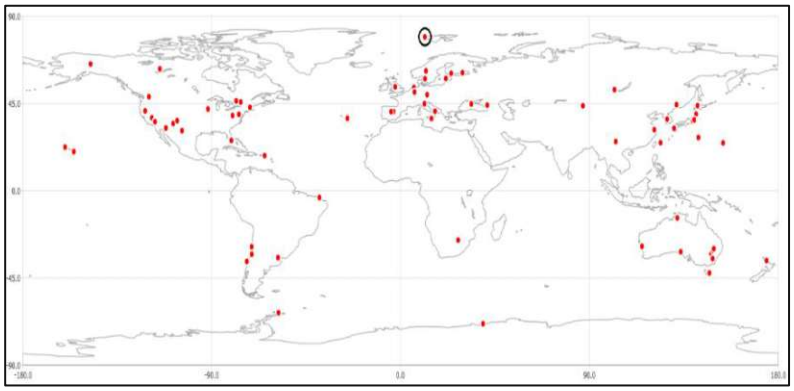

Figure 3.1. VLBI network, where the northernmost dot marks the Ny-Alesund Observatory (VieSched++ Screenshot).

Figure 3.2. picture of the Nyales20 telescope (Garcia-Espada et al., 2022).

"In 2021/2022, the 20-m Ny telescope was scheduled for 243 24-hour VLBI observations, including R1, R4, EURO, RD, and RDV sessions, along with 64 one-hour observations within the intensive program. Despite a five-month downtime from June to October 2021 due to technical issues. The telescope faced additional problems in October and November 2022" (Garcia-Espada et al., 2022).

Despite its technical issues, Nyales20 continued to co-exist and operate for some time alongside Nyale13S to link ITRF and ICRF, respectively

Since the Ny-Alesund Observatory is the most northerly located observatory, it pays an essential role because it can register the effects of climate change clearly as well as earlier than other observatories (*web: craf.eu*).

According to (Garcia-Espada et.al., 2022) in Arctic, region of several large glaciers, has been confirmed that Svalbard's glaciers are losing mass due to climate change, which created a challenge for the stability of the reference frame.

Therefore, the construction of a new station, namely the twin VGOS Nyale13s and Nyale13n telescopes at Brandal, a few kilometres further north, began in 2013. It was officially opened in 2018 and has been operational since 2020.

They are located at the Ny-Alesund Observatory, surrounded by the Brandal Lagoon, Cape Mitra and Kings Fjord, and are 13.2 meters in diameter. They co-locate the four essential space geodetic techniques, namely SLR, DORIS, GNSS and VLBI.

The Ny-Alesund North antenna (Nn) has participated in the VGOS network since August 2022, whereas the south antenna (Ns) has been part of the legacy S/X network since 2020. The installation of a VGOS receiver is planned for the end of 2024 (Garcia-Espada et al., 2022).

"The 13-m Ns telescope has participated in 247 24-hour VLBI sessions, including R1, R4, EURO, RD, T2, and RDV sessions, as well as 57 one-hour sessions within the Intensive Program; furthermore, the 13-m the Nyale13N telescope started operations in August 2022 and was designed as a core station in the VGOS VLBI network" (Garcia-Espada et al., 2022).

Table 3.2 presents characteristics of the VGOS Nyale13s and Nyale13n telescopes:

	Nyale13S	Nyale13N
geographic longitude:	11° 51′ 17″	11° 51′ 19″
geographic latitude:	78° 56′ 36″	78° 56′ 33″
diameter telescope:	13.2m	13.2m
minimum elevation:	0°	0°

Table 3.2. Basic information about Nyale13S and Nyale13N radio telescope (see website: CRAF-Committee on Radio Astronomy Frequencies).

Figure 3.3. VGOS Twin telescopes Nyale13s and Nyale13n (Garcia-Espada et al., 2022).

Table 3.3 provides a comprehensive comparison of VGOS and legacy systems:

	Legacy S/X System	**VGOS System**	**Benefit**
Antenna size	5- 100 m dish	12-13 m dish	Reduced cost
Slew Speed	~20-200 deg/min	≥ 360 deg/min	More observations for the troposphere
Sensitivity	200-15,000 SEFD	≤ 2,500 SEFD	More homogeneous
Frequency Range	S/X band (two bands)	2-14 GHz (four bands)	Increased sensitivity & data precision
Recording Rate	128, 256, 512 Mbps	8, 16, 32 Gps	Increased sensitivity
Data Transfer	usually e-transfer, some ship disks	e-transfer, ship disk when required	
Signal Processing	analog/digital	digital	Stable instrumentation

Table 3.3. Comparison between legacy system and VGOS (see website: CRAF-Committee on Radio Astronomy Frequencies).

Table 3.4 presents frequency bands for the legacy system and VGOS:

Observing mode	Frequency band
20m VLBI	2200 – 2370 MHz
20m VLBI	3220 – 3390 MHz
20m VLBI	4800 – 6700 MHz
20m VLBI	8150 – 8650 MHz
13m IVS VGOS	**2 – 14 GHz**

Table 3.4. Frequency bands used for the legacy system and VGOS (see website: CRAF-Committee on Radio Astronomy Frequencies).

The twin telescopes will be part of the next-generation VGOS network, which aims to improve the accuracy and precision of VLBI data. The VGOS twin telescopes will be able to observe two sources simultaneously, allowing for more efficient data acquisition. Additionally, the fast-slewing antennas will enable the telescopes to rapidly switch between sources, thereby further increasing the efficiency of data acquisition (Schuh & Böhm, 2013). This network is being developed to be minimally staffed and remotely controllable.

Ny-Alesund is among the core sites within the GGOS, which is a fundamental part of a telescope network that defines the global geodetic reference frame. It is crucial to realizing GGOS's ambitious goals of 1mm accuracy and 0.1mm/year stability (Schuh & Böhm, 2013).

In conclusion, the transition from VLBI2010 to VGOS represents a critical advancement in space geodetic techniques. The adaption of new technological advancements aims to realize the ambitious geodetic goals of 1mm accuracy and 0.1mm/year stability (Schuh & Böhm, 2013).

4. Methodology

The fourth Chapter outlines the data utilized for our analysis. Additionally, it describes the concept of VieVS and its workflow for this case study. Lastly, it provides an explanation about VieSched++ software.

4.1. Provided data

The analysis for this project was conducted using real data provided by the IVS (see chapter 2.3) between 2020 and 10/2022.

This section provides a brief description of each data type of the sessions used for this case study, specifically R1, R4, RD, RV, and T2 sessions. The data were directly downloaded in the open-source vgosDB format, which is the IVS standard format for storing, transmitting, and archiving VLBI data (example: 20APR01XA.tgz; 20APR08XA.tgz etc.).

Table 4.1 explains the meaning of vgosDB file nomenclature:

CODE	Meaning
YY	2- digit year
MMM	3-character month (APR)
DD	2-digit day
XX	2-character indicating the particular session
.tgz	gzipped tar file

Table 4.1. Meaning of the vgosDB file (NASA Earth Data – CDDIS VLBI level 2 vgosDB format data).

In the following sections, a brief explanation of the VLBI sessions (R1, R4, T2, RD, RV) is provided.

4.1.1. IVS - sessions: R1 and R4

The goal of the IVS-R1 and IVS-R4 sessions is to provide bi-weekly EOP results through VLBI regularly. The letter “R’” stands for rapid turnaround, while the numbers “1” and “4” indicate the day of the week where the measurements are scheduled, specifically “Mondays” and “Thursdays” (Lambert et al., 2006).

R1 session data should reach the correlator center no later than Friday, while data from R4 session sshould be shipped as early as possible on Monday, with an arrival target no later than Thursday.

These sessions began in January 2002 with a network of five to six stations and increased over time to a network size of 11 to 13 stations in 2017 (Thomas et al., 2018).

The R1 network allows very long east - west baselines (America - Europe and Europe - Japan, whereas the R4 network is significantly smaller, covering approximately a third of the Earth's surface (Lambert et al., 2006).

4.1.2. IVS-Sessions : T2 and RDV

IVS-T2 primarily focuses on performing bi-monthly VLBI sessions to consistently monitor TRF. By contrast, IVS-RDV sessions encompass a diverse range of coordinated astronomical and geodetic experiments that occur twice a month using the complete set of VLBA stations (*IVS web site*).

These experiments are organized by the geodetic VLBI programs of the following three agencies:

- U.S. Naval Observatory (USNO);
- National Aeronautics and Space Administration (NASA);
- National Radio Astronomy Observatory (NRAO).

4.1.3. GNSS time series

We used GNSS time series data, openly available from the Nevada Geodetic Observatory's official web-site (*Blewitt et al., (2018)*), specifically focusing on the NYA2 Station in Ny-Alesund.

The laboratory is situated in Nevada, and its primary objective is to investigate scientific issues within space geodesy at regional and global scales. It employs the Global Positioning System (GPS) to analyze tectonic activity in Nevada. Additionally, its global-scale studies encompass research on surface mass loading and global-scale plate tectonic issues (*Nevada Geodetic Laboratory*).

4.2. General concepts of VieVS

VieVS is a analysis software for geodesy and astrometry. The software was developed by the Institute of Geodesy and Geophysics (IGG), Vienna University of Technology. It's written in MATLAB, which has the advantage of being easy to use and source code can be applied without much effort (Böhm et al., 2018).

VieVS software was used to analysing our data from VLBI observations.

The main modules of the VieVS are as follows:

- VIE INIT (Initialising): This module is responsible for reading the data provided in vgosDB format, and the created data are stored in the LEVEL 0 folder.
- VIE MOD (modeling): This module's task is to calculate theoretical delays and its partial derivatives. The data created here are stored in the LEVEL 1.
- VIE LSM (Least Squared Method – parameter estimation): This module is responsible for parameter estimation, such as EOPs, station, source coordinates and clock offsets. The results are stored in the LEVEL 3 folder for further investigation (Böhm et al., 2018).

In addition, there are also other modules, namely VIE SIM and VIE GLOB, which are described as follows:

- VIE SIM (Simulation): This module is responsible for the creation of simulated observations for an observation plan (which could either be from real sessions or scheduled ones). To create a realistic observation, this module combines the theoretical delay with simulated values for zenith wet delay, clocks, and observation noise at each epoch. The simulated value, namely NGS file, can then be analysed with the main VieVS methods.
- VIE GLOB (GLOBAL): This module combines the normal equations of several sessions into a global solution to calculate reference frames and global parameters (Schuh & Böhm, 2013).

Figure 4.1 displays the structure of VieVS software:

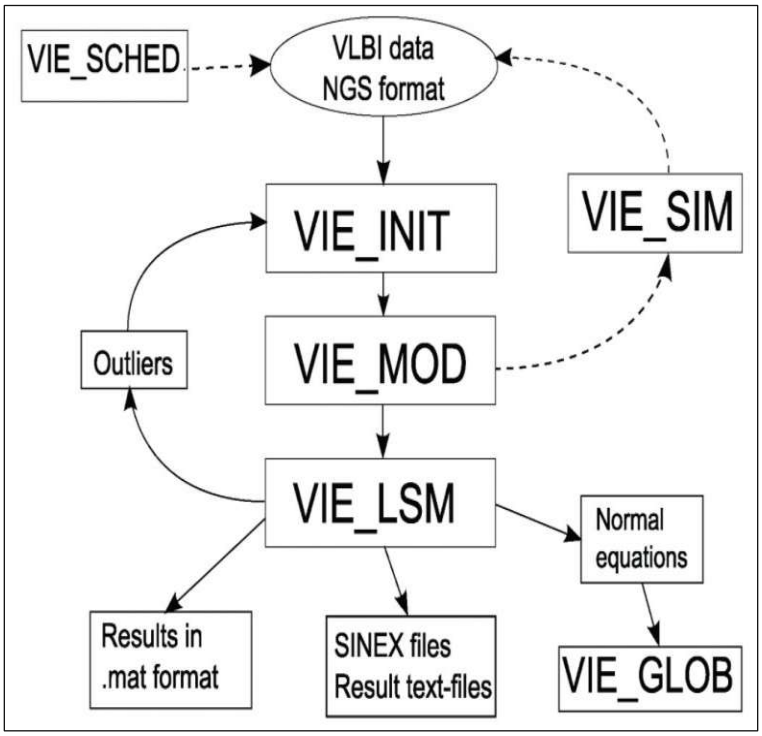

Figure 4.1. Structure of VieVS's Old Flow Chart (VieVS Wiki).

4.2.1. Further elaboration of Vie_LSM Module.

The VIE_LSM module is a crucial part of VieVS. It utilizes the LSM to estimate unknown parameters within an overdetermined system of equations. In essence, the LSM connects observations, often denoted as (l), to various unknown parameters. These parameters can include station positions, EOPs, source positions, tropospheric information, and more. The ideal scenario for employing the LSM is when observations follow a normal distribution, which indicates that there are no large sources of error or that any existing errors have been effectively addressed before the estimation process (Navratil. G., 2020).

According to Schuh (2020) before parameter estimation takes place, the raw observations must be cleaned from several systematic effects, that limit the final accuracy of the results.

Figure 4.2. provides a visual representation of the fundamental concept behind the VLBI data analysis algorithm VIE_LSM. It depicts how the observed and computed values converge in a single least squares adjustment (LSM). In this process, the reduced observed delay and theoretical delay come together, enabling the estimation of unknown parameters within an overdetermined system of equations (Schuh & Böhm, 2013).

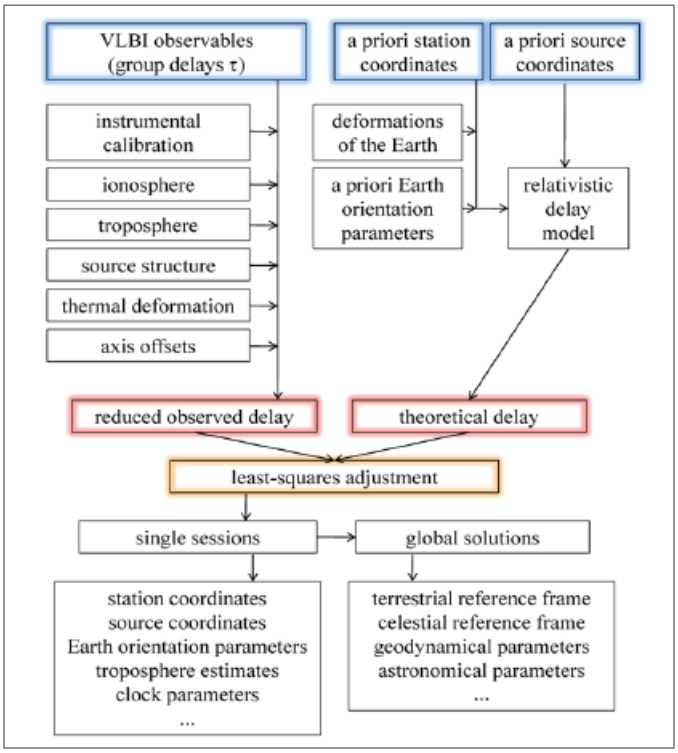

Figure 4.2. Structure of the VIE_LSM Module (Schuh & Böhm, 2013).

The analysis comprises two main streams: One processes actual observations with corrections for instrumental and environmental factors, resulting in the reduced observed delay, while the other stream generates theoretical delays based on a priori parameters values. These streams converge at the parameter estimation algorithm, where the formation of “observed minus computed” values occurs, allowing for the estimation of unknown parameters. These parameters can include station coordinates, EOPs, clock parameters, troposphere and ionosphere parameters depending on whether one is working on a single or global solution.

The LSM can be applied at two levels, namely a single solution or a global solution, the products of which are presented in Table 4.1:

Single Solution	**Global Solution**
Station Coordinates	TRF
Source Coordinates	CRF
EOP	Geodynamical Parameters
Troposphere Estimation	Astronomical Parameters
Clock Parameters	…

Table 4.1. Products of a single and a global solution.

As seen in Table 4.1, the estimated parameters of the single solution include station coordinates, source coordinates, Earth orientation parameters (EOP), tropospheric parameters, and clock parameters. To simplify the estimation process, VieVS uses Continuous Piecewise Linear Offsets (PWLO) to reduce the number of estimated parameters. These parameters are estimated at specific time intervals, such as every 15, 30 or 60 minutes, between which linear interpolation is used.

By generating additional values as PWLOs, the number of observations increases, which is essential because the LSA requires more observations than unknowns for reliable results. This approach is useful when dealing with numerous unknown parameters, such as troposphere parameters (specifically ZWD and, gradients) and clock parameters.

Since there are many of unknown parameters, PWLOs help to reduce the number of estimated parameters.

To illustrate Figure 4.3, we estimate parameters at times t1 & t2. Between them, by using a linear interpolation method, new values (t) could be generated. Since PWLOs are time-dependent, the new value (t), for instance, can be generated every 15, 30 or 60 minutes.

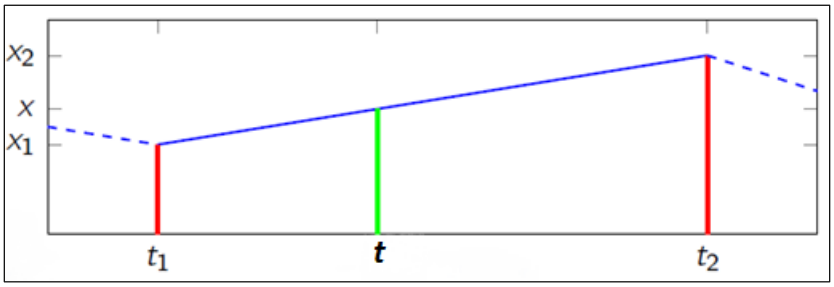

Figure 4.3. Basic Principle of Interpolating New PWLO values (B*öhm, 2021*).

Constraints can be introduced to enhance the accuracy of estimations and avoid singularities.

There are two types of constraints, namely relative and absolute constraints:

Relative constraints fill gaps in observations within an estimation interval and ensure that the next estimated parameter does not deviate significantly from the previous one, maintaining the regularity of the normal equation (Matrix N).

Absolute constraints are applied when a preferred parameter value is known, and they limit the estimated value to a certain range from the a priori expectation. For example, an absolute constraint may restrict the value at 03:00 to be within 1.5cm of the value at 04:00.

In summary, the VIE_LSM module uses the least squares method to estimate unknown parameters based on observed and computed values, with the help of CPWLO.

4.2.2. Workflow in VieVS

First, we used the MATLAB function mk_list (*mk_list('R1','REQSTAT', 'NS')*) to separate each session (R1, R4, RD, RV, and T2). This was done for all sessions separately.

Then, we parametrized the process lists to start our analysis using VieVs.

- Reference frames:
  - CRF fixed to ICRF3;
  - TRF fixed to ITRF2014.

- Clock estimation (least squares):
  - Clock breaks were used from OPT file;
  - Clocks were estimate (pwl offset, one rate & one quadratic term per clock);
  - Relative constraints were introduced between pwl clock offsets (1.3cm after 60min);
  - The baseline-dependent clock offset was estimated (according to OPT file).

- VieVS estimation settings:
  - Run first solution (one offset, ore rate & one quadratic term per clock);
  - Run main solution – parameter estimation (Simple outlier test (c*m0)), c=5;
  - Introduce elevation dependent noise.

Next, we checked the residuals of the first solution for each session separately. If there was a jump in the residuals, we used clock breaks to fix it.

Afterwards, we checked the residuals again for all sessions to identify any obvious outliers and mark them.

Finally, by using the VieVS function “stat_coo_out”, the station coordinates for each session from 2020 to 10/2022 were exported (see Figure 4.4).

XYZ_dHEN_Final_R1_NS.txt

```
#col 1: station
#col 2: mjd of the session
#col 3-5: a priori XYZ [m]
#col 6-8: estimated XYZ [m]
#col 9-11: formal errors of estimated XYZ [m]
#col 12-14: dHEN w.r.t. a priori [m]
#col 15-17: formal errors of dHEN [m]
#col 18: session
#

HART15M     59346    5085490.7919    2668161.6525   -2768692.4824     5085490.7848    2668161.6476   -2768692.4715     0.0118    0.0072    0.0099    -0.0124    -0.0010
NYALES20    59346    1202462.4040     252734.5831    6237766.2964     1202462.4133     252734.5608    6237766.3188     0.0077    0.0057    0.0251     0.0228    -0.0237
SEJONG      59346   -3110080.2419    4082066.5777    3775076.7366    -3110080.2334    4082066.5801    3775076.7168     0.0075    0.0095    0.0105    -0.0145    -0.0082
WETTZ13N    59346    4075627.5314     931774.4126    4801552.4470     4075627.5323     931774.4247    4801552.4430     0.0082    0.0061    0.0111    -0.0006     0.0116
YARRA12M    59346   -2388896.5261    5043350.0663   -3078590.4347    -2388896.5377    5043350.0790   -3078590.4441     0.0110    0.0130    0.0118     0.0189     0.0051
BR-VLBA     59242   -2112065.3227   -3705356.5035    4726813.6132    -2112065.3232   -3705356.5106    4726813.6215     0.0009    0.0015    0.0018     0.0105     0.0030
FD-VLBA     59242   -1324009.4265   -5332181.9439    3231962.3507    -1324009.4299   -5332181.9458    3231962.3493     0.0006    0.0017    0.0010     0.0015    -0.0029
HN-VLBA     59242    1446374.7403   -4447939.6895    4322306.2160     1446374.7354   -4447939.6824    4322306.2083     0.0007    0.0014    0.0014    -0.0113    -0.0025
LA-VLBA     59242   -1449752.6969   -4975298.5660    3709123.7994    -1449752.6984   -4975298.5632    3709123.7967     0.0010    0.0025    0.0017    -0.0035    -0.0023
MK-VLBA     59242   -5464075.2896   -2495247.6054    2148297.6118    -5464075.2790   -2495247.6030    2148297.6073     0.0022    0.0019    0.0014    -0.0116     0.0023
NL-VLBA     59242    -130872.6212   -4762317.0803    4226850.9808     -130872.6233   -4762317.0745    4226850.9761     0.0005    0.0013    0.0011    -0.0074    -0.0022
NYALE13S    59242    1201070.5952     252129.3527    6238022.5548     1201070.5982     252129.3554    6238022.5542     0.0018    0.0015    0.0048     0.0001     0.0020
ONSALA60    59242    3370605.6831     711917.8376    5349830.9817     3370605.6820     711917.8403    5349830.9800     0.0016    0.0010    0.0021    -0.0017     0.0029
OV-VLBA     59242   -2409150.5469   -4478573.0616    3838617.3033    -2409150.5530   -4478573.0764    3838617.3076     0.0010    0.0017    0.0013     0.0153     0.0017
PIETOWN     59242   -1640954.0508   -5014816.0182    3575411.7434    -1640954.0526   -5014816.0214    3575411.7497     0.0006    0.0015    0.0010     0.0065    -0.0007
WETTZELL    59242    4075539.4994     931735.6757    4801629.6071     4075539.5072     931735.6791    4801629.6116     0.0017    0.0011    0.0021     0.0089     0.0016
BR-VLBA     59403   -2112065.3290   -3705356.5033    4726813.6098    -2112065.3342   -3705356.5068    4726813.6136     0.0015    0.0021    0.0027     0.0065    -0.0028
FD-VLBA     59403   -1324009.4320   -5332181.9436    3231962.3486    -1324009.4381   -5332181.9480    3231962.3452     0.0017    0.0028    0.0024     0.0032    -0.0049
HARTRAO     59403    5085442.7560    2668263.9582   -2768696.6089     5085442.7835    2668263.9749   -2768696.6347     0.0184    0.0135    0.0132     0.0402     0.0020
HN-VLBA     59403    1446374.7335   -4447939.6902    4322306.2179     1446374.7292   -4447939.6823    4322306.2065     0.0015    0.0025    0.0027    -0.0143    -0.0016
HOBART26    59403   -3950237.6902    2522347.7498   -4311561.5318    -3950237.6865    2522347.7289   -4311561.5264     0.0116    0.0113    0.0158    -0.0142     0.0157
KP-VLBA     59403   -1995678.9524   -5037317.6868    3357327.9637    -1995678.9631   -5037317.6968    3357327.9686     0.0017    0.0022    0.0022     0.0138    -0.0063
LA-VLBA     59403   -1449752.7031   -4975298.5657    3709123.7972    -1449752.7073   -4975298.5687    3709123.7959     0.0015    0.0022    0.0022     0.0026    -0.0032
MK-VLBA     59403   -5464075.2961   -2495247.5779    2148297.6264    -5464075.3090   -2495247.5860    2148297.6231     0.0034    0.0026    0.0027     0.0131     0.0020
NYALE13S    59403    1201070.5896     252129.3552    6238022.5593     1201070.5948     252129.3548    6238022.5883     0.0032    0.0024    0.0098     0.0294    -0.0014
ONSALA60    59403    3370605.6768     711917.8441    5349830.9863     3370605.6862     711917.8462    5349830.9862     0.0026    0.0018    0.0039     0.0051     0.0002
OV-VLBA     59403   -2409150.5549   -4478573.0586    3838617.3017    -2409150.5604   -4478573.0730    3838617.3049     0.0017    0.0023    0.0023     0.0140     0.0020
PIETOWN     59403   -1640954.0569   -5014816.0181    3575411.7411    -1640954.0534   -5014816.0130    3575411.7391     0.0016    0.0024    0.0023    -0.0061     0.0018
SC-VLBA     59403   -2607848.7055   -5488969.4637    1937739.8411    -2607848.6975   -5488969.4563    1937739.8307     0.0024    0.0040    0.0027    -0.0138    -0.0041
```

Figure 4.4. Screenshot illustrating the results generated by sing VieVS.

Figures 4.5 and 4.6 were generated, which display the formal errors for the station Nyales20 and Nyale13s during the study period gained after the VieVS analysis:

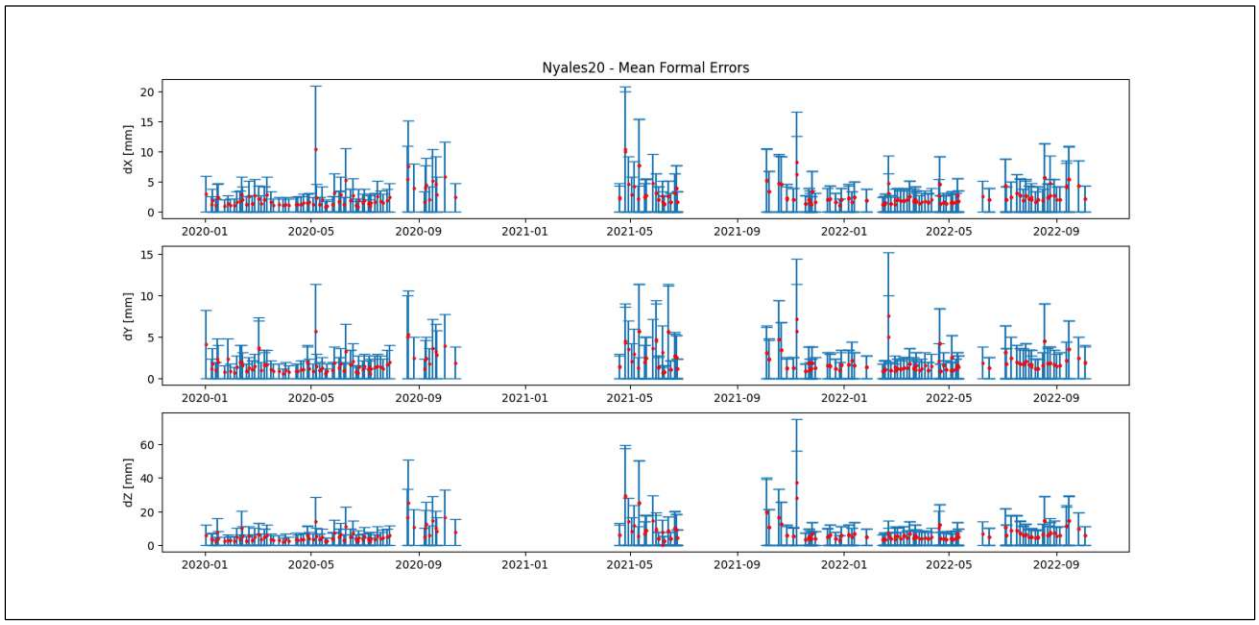

Figure 4.5. Formal errors of estimated XYZ of the station Nyales20 after VieVS analysis.

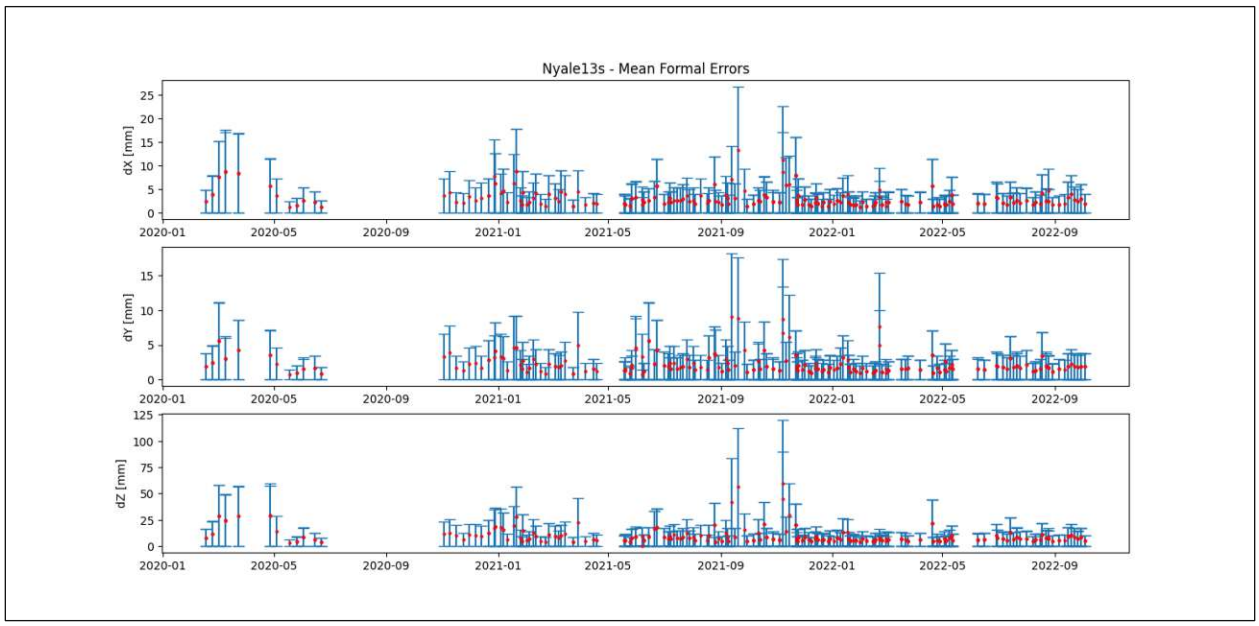

Figure 4.6. Formal errors of estimated XYZ of the station Nyale13s after VieVS analysis.

4.3. General concepts of Vieschedpp++

VieSched++ is a software tool used for scheduling VLBI observations, primarily for geodesy and astrometric purposes. It is a standalone tool of VieVS developed at the Technical University of Vienna (TU Wien) and consists of two main components, namely a scheduler and a graphical user interface (GUI). The GUI assist in creating the necessary .xml documents for scheduling and offers additional features like schedule analysis and comparisons between different schedules and station log files (Schartner & Böhm, 2019).

This software allows for various optimization criteria, including sky coverage, scan duration, number of observations, idle time, average station usage, average source usage, average baseline usage, low elevation, and low declination. Choosing the right combination of optimization criteria and their weighting factors is crucial for creating an efficient schedule (*Schartner et al.2017*).

Sky coverage is an essential parameter because it helps to reduce tropospheric errors, a significant source of error in VLBI observations. The more the sky is covered with observations, the more accurately the tropospheric parameters can be estimated. However, focusing excessively on sky coverage can result in longer slewing times for the telescopes, thus reducing the number of observations (Schartner & Böhm, 2019).

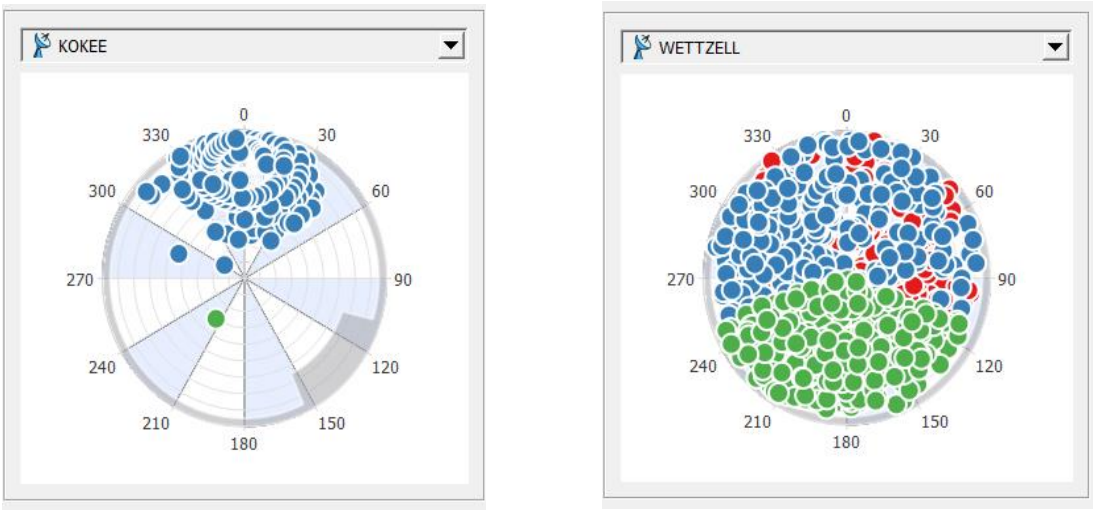

Figure 4.7. Sky coverage scenario in VieSched++.

Duration is another critical optimization criterion. Longer observation times are required to achieve a valid Signal-to-Noise Ratio (SNR) in VLBI observations. This is because longer observations result in more accurate SNR values. The SNR can be improved by using more sensitive stations, higher recording rates, and stronger sources. The duration of observation is determined based on various factors, including station sensitivity (SEFD), the SNR, source brightness, recording rate, and source flux density (Schartner & Böhm, 2019)..

Balancing the number and distribution of observations is challenging. One can either acquire a higher number of observations with poorly distributed coverage or have well-distributed observations with fewer numbers. Finding a compromise between these factors is essential for achieving the best results (Schartner & Böhm, 2019).

In addition, the so-called Multi-Scheduling Tool is crucial to mention. It is a very powerful feature in VieSched++ that generates multiple schedules with different optimization criteria. This tool helps create an optimized schedule with customized parameters and allows for the generation of a large number of schedules (up to 9999). It uses a brute-force algorithm to evaluate schedules based on criteria such as sky coverage, scan duration, and the number of observations. The software suggests the best schedule and alternative schedules based on weight factors (Schartner, 2018).

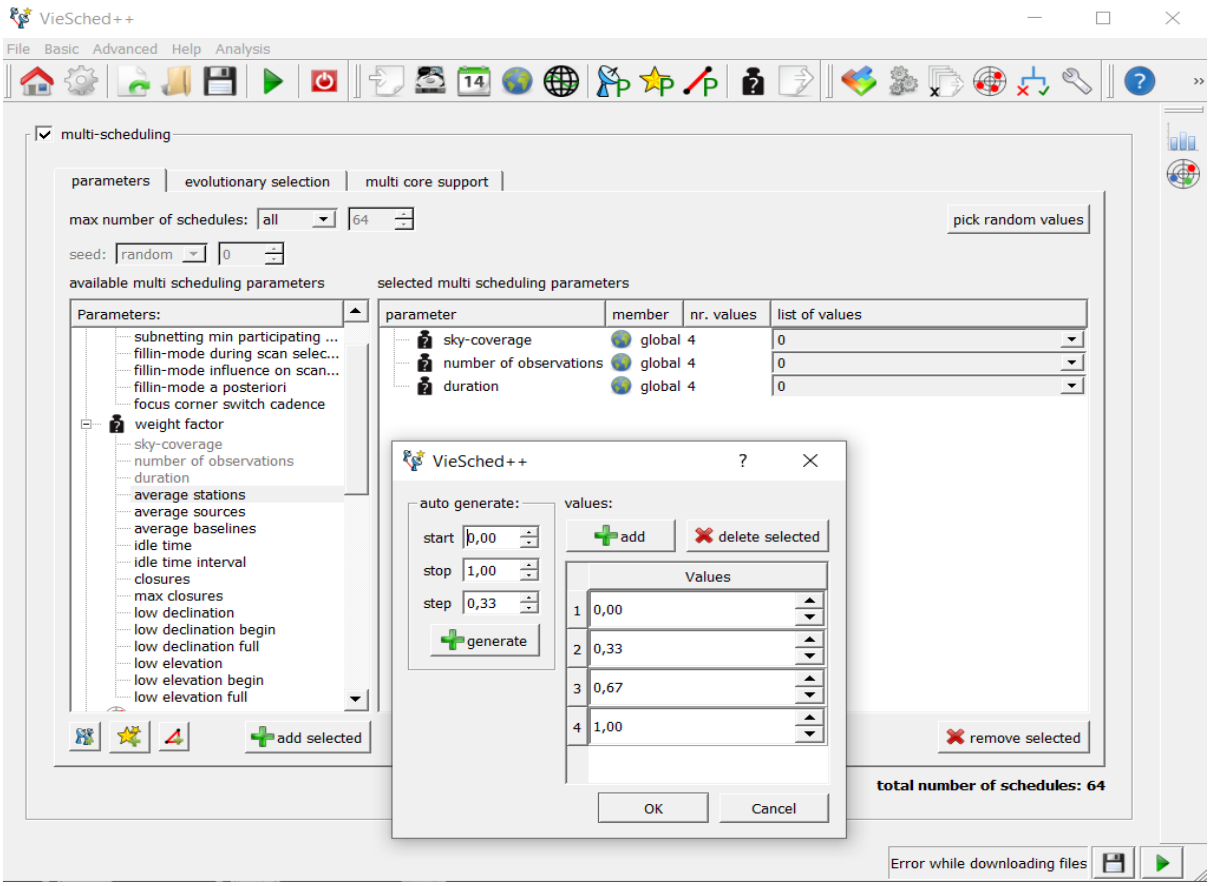

Figure 4.8. Weighting factors in VieSched++.

In the process of scheduling, we primarily aimed to determine the number of observations and the quality of their distribution. However, assessing the quality of our estimated geodetic parameters was potentially complex. To address this, Viesched++ offers a simulation feature that allowed us to test our scheduling choices and demonstrate the quality of the estimated parameters.

These simulations assist in evaluating the mean formal errors and repeatability of geodetic parameters. Depending on the session duration, different parameters can be estimated, such as geodetic parameters and Earth Orientation Parameters (EOP). Simulations are especially valuable in assessing the quality of estimated parameters in different types of VLBI sessions.

Following chapter gives a detailed explanation about the parameter estimation method, that was used for this study case.

5. Parameter estimation – Gauss-Markov Model

This chapter offers a detailed explanation about Gauss-Markov parameter estimation method which was used to estimate the linear equation coefficients (x_{Ny}, x_{Ns} and x_{NYA2}) representing velocities.

Additionally, it gives an explanation about the linear regression model, which was used to determine v1 and v2 parameters, indicating the initial and final coordinates for each dimension (X, Y, and Z) during the study period for all participating stations, namely Nyales20, Nyale13s, and NYA2.

These parameters together with the Modified Julian Date (mjd: first and last session) were subsequently utilized to fit the linear regression model into given data, namely timeseries.

5.1 Parameter estimation

There are various methods for parameter estimation, including the Kalmar Filter, least-squares collocation, and square-root information filters. These approaches treat atmospheric and clock variations as stochastic processes the Gauss-Markov model, based on standard least-squares adjustments (Nothnagel et.al. 2023).

In this case study, we firstly examined the stochastic model of the observations. Though this step, we determined the weight, that each observation contributed to the least-squares adjustment.

Thereafter, we ran the Gauss-Markov model to estimate required parameters.

5.1.1 Stochastic model

The foundation of the VLBI stochastic model lies in the standard deviation or variance of observations. In our case, these values were calculated based on the formal errors in the three respective axes (x, y, and z) and placed in diagonal order in their respective matrices.

The resulting covariance matrices for both stations ($P_{x,}$ P_y, P_z) contained the stochastic nature of the observations, whereas ($\sigma_x, \sigma_y, \sigma_z$) represent the formal errors in each respective axis.

- P_x matrix:

$$P_x = \begin{pmatrix} \frac{1}{\sigma^2 \mathrm{xi}} & 0 & \dots & 0 & 0 \\ 0 & \frac{1}{\sigma^2 \mathrm{xj}} & 0 & 0 & 0 \\ \vdots & 0 & \ddots & 0 & \vdots \\ 0 & 0 & 0 & \frac{1}{\sigma^2 \mathrm{x}m} & 0 \\ 0 & 0 & \dots & 0 & \frac{1}{\sigma^2 \mathrm{xn}} \end{pmatrix}$$

- P_y matrix:

$$P_y = \begin{pmatrix} \frac{1}{\sigma^2 yi} & 0 & \dots & 0 & 0 \\ 0 & \frac{1}{\sigma^2 yj} & 0 & 0 & 0 \\ \vdots & 0 & \ddots & 0 & \vdots \\ 0 & 0 & 0 & \frac{1}{\sigma^2 ym} & 0 \\ 0 & 0 & \dots & 0 & \frac{1}{\sigma^2 yn} \end{pmatrix}$$

- P_z matrix:

$$P_z = \begin{pmatrix} \frac{1}{\sigma^2 \mathrm{z}i} & 0 & \dots & 0 & 0 \\ 0 & \frac{1}{\sigma^2 \mathrm{zj}} & 0 & 0 & 0 \\ \vdots & 0 & \ddots & 0 & \vdots \\ 0 & 0 & 0 & \frac{1}{\sigma^2 \mathrm{z}m} & 0 \\ 0 & 0 & \dots & 0 & \frac{1}{\sigma^2 \mathrm{z}n} \end{pmatrix}$$

5.1.2 Gauss-Markov Model

Expressed as $y = A \cdot \mathrm{x} + \mathrm{v}$, the classical least-squares adjustments in a Gauss Markov model involve vectors y (abbreviated observations), x (unknown parameters), and v (residuals; Nothnagel et.al. 2023).

The linearized design matrix A was formed from the independent variable values (in this case, $\frac{mjd_i - mjd_0}{365.25}$).

- $A\ Matrix$ (Order of 336 x 2)

$$A = \begin{pmatrix} \frac{mjd_i - mjd_0}{365.25} & 1 \\ \frac{mjd_j - mjd_0}{365.25} & 1 \\ \vdots & \vdots \\ \frac{mjd_m - mjd_0}{365.25} & 1 \\ \frac{mjd_n - mjd_0}{365.25} & 1 \end{pmatrix}$$

The elements of the first column in matrix A were computed using the equation $\left(\frac{mjd_i - mjd_0}{365.25}\right)$, where mjd_i represents the Modified Julian Date on which the session took place, starting from the first session and mjd_0 is set to 57023 for VLBI stations Nyales20 and Nyale13s, indicating the reference epoch of ITRF2020 (January 1, 2015). By contrast, for the GNSS data $mjd_0 = 58849$ indicated first session of our study period specifically corresponding to January 1, 2020.

The normal equation system $N \cdot x = b$ was solved, with N being the normal equation matrix, and b representing the right-hand side (Nothnagel et.al. 2023).

The normal equation system was as follows:

$$N = (A^{\mathrm{T}} \Sigma \mathrm{yy}^{-1} \cdot A) \qquad (5.1)$$

The right-hand side of the Normal equation was solved as follows: $b = (A^{\mathrm{T}} \cdot \Sigma \mathrm{yy}^{-1} \cdot y)$ (5.2),

where y contains the estimated coordinates of the session.

The following matrices (b_x, b_y, b_z) contain b vectors of our solution.

- Station Nyales20:

$$\begin{aligned} b_x &= (7.70515377\mathrm{e}+14 \quad 1.27188550\mathrm{e}+14) \\ b_y &= (1.61947582\mathrm{e}+14 \quad 2.67325981\mathrm{e}+13) \\ b_z &= (3.99704375\mathrm{e}+15 \quad 6.59789814\mathrm{e}+14) \end{aligned}$$

- Station Nyale13s:

$$\begin{aligned} b_x &= (5.16927695\mathrm{e}+14 \quad 7.68304117\mathrm{e}+13) \\ b_y &= (1.08513727\mathrm{e}+14 \quad 1.61282795\mathrm{e}+13) \\ b_z &= (2.68477695\mathrm{e}+15 \quad 3.99035534\mathrm{e}+14) \end{aligned}$$

- GNSS Station NYA2:

$$\begin{aligned} b_x &= (2.75818698\mathrm{e}+15 \quad 1.81408339\mathrm{e}+15) \\ b_y &= (5.79162032\mathrm{e}+14 \quad 3.80919863\mathrm{e}+14) \\ b_z &= (1.4309114\mathrm{e}+16 \quad 9.4112278\mathrm{e}+15) \end{aligned}$$

Finally, the linear equation $N \cdot x = b$ was solved to obtain the vector of estimated parameters x.

The vector of the estimated parameters **x** was then computed with:

$$(A^{\mathrm{T}} \cdot \Sigma \mathrm{yy}^{-1} \cdot A) \cdot x = (A^{\mathrm{T}} \cdot \Sigma \mathrm{yy}^{-1} \cdot y) \qquad (5.3)$$

The least squares solution was calculated, where $(A^{\mathrm{T}} \cdot \Sigma \mathrm{yy}^{-1} \cdot A)$ is part of the least squares problem formulation. The vector (b) was on the right-hand side of the linear equation (Nothnagel et.al. 2023).

As we can see, the results of the linear equations, namely first raw of Matrixes x_{Ny}, x_{Ns} and x_{NYA2}, contain velocities in mm/year, specifically position change of each axis (X, Y, and Z) in mm per year.

- Station Nyales20:

$$x_{Ny} = \begin{pmatrix} \mathbf{-1.46307826e-02} & \mathbf{6.97224682e-03} & \mathbf{1.32648309e-02} \\ 1.20246250e+06 & 2.52734536e+05 & 6.23776623e+06 \end{pmatrix}$$

- Station Nyale13s:

$$x_{Ns} = \begin{pmatrix} \mathbf{-1.49488456e-02} & \mathbf{5.17453479e-03} & \mathbf{1.25649325e-02} \\ 1.20107069e+06 & 2.52129319e+05 & 6.23802249e+06 \end{pmatrix}$$

- GNSS Station NYA2:

$$x_{NYA2} = \begin{pmatrix} \mathbf{-1.45948844e-02} & \mathbf{7.35777614e-03} & \mathbf{1.17643043e-02} \\ 1.20237928e+06 & 2.52474679e+05 & 6.23778658e+06 \end{pmatrix}$$

The velocities in mm/year for the VLBI stations Nyales20 and Nyale13s, as well as the GNSS site NYA2, were as follows:

- *NY: [vx, vy, vz]: [-14.6, 7.0, 13.3] mm/year*
- *NS: [vx, vy, vz]: [-15.0, 5.2, 12.6] mm/year*
- *NYA2: [vx, vy, vz]: [-14.59, 7.36, 11.76] mm/year*

5.2 Linear Regression

Linear regression is a statistical approach, which assumes that there is approximately a linear relationship between to variables, namely X and Y (James et.al, 2023).

Mathematically, it can be written as follows:

$$Y \approx \beta_0 + \beta_1 X \qquad (5.4)$$

Where:

$\beta_0 \; and \; \beta_1$ – estimated coefficients (in our case coefficients of linear equation, x_{Ny}, x_{Ns} and x_{NYA2})
$Y \; and \; X$ – Prediction of Y ((v_i) on the basis of X - indicating MJD.

Figure 5.1 shows that linear regression model involves two variables: Y and X. We are interested in the distribution of the random variable Y (v_1, v_2) depending on X (the independent variable – MJD).

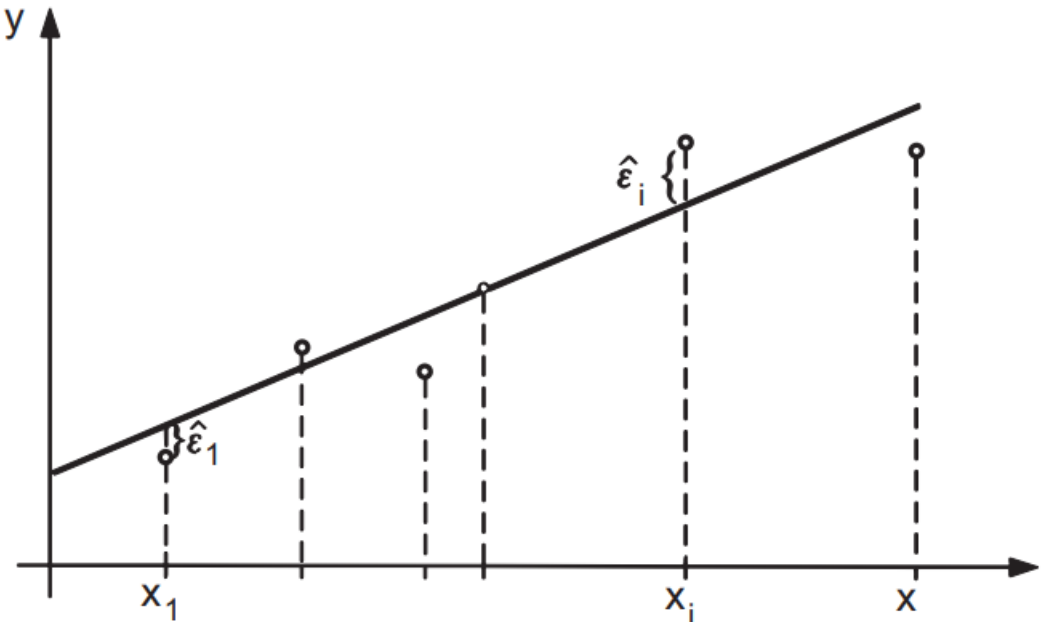

Figure 5.1 Linear regression, relationship between variables X and Y (Navratil, G., 2020).

The following lists, (v_1) the initial and (v_2) final coordinates, indicating predictions (Y) see equation 5.4:

- Station Nyales20:

  v_1: [1202462.4261717678, 252734.57066550915, 6237766.293866761]
  v_2: [1202462.3863151527, 252734.58965903573, 6237766.330002303]

- Station Nyale13s:

  v_1: [1201070.609525715, 252129.34583351112, 6238022.549834038]
  v_2: [1201070.5702351145, 252129.3594339311, 6238022.582858912]

- GNSS station NYA2:

  v_1: [1202379.2788489598,252474.67869142964,6237786.583771794]
  v_2: [1202379.238570675, 252474.69899707878, 6237786.616238375]

On the other hand, (mjd_0), time when the first session took place and (mjd_{-1}) last session, both indicating the independent variable X (see equation 5.4), which were used to determine the linear regression model.

- Station Nyales20:
  - mjd_0 : [58862 indicating January 14, 2020]
  - mjd_{-1}: [59857 indicating October 05, 2022]
- Station Nyale13s:
  - mjd_0 [58897 indicating February 18, 2020]
  - mjd_{-1} [59857 indicating October 05, 2022]
- Station GNSS-NYA2:
  - mjd_0 [58849 indicating January 1, 2020]
  - mjd_{-1} [59857 indicating October 5, 2022]

Following chapter exhibits the results of our study, also including the absolute positions for the stations Nyales20, Nyale13s and NYA2 over the study period, accompanied by a simple linear regression line.

6. Results

In this chapter, were presented the results of our comprehensive analysis of the VLBI station data from Nyales20 and Nyale13s. The aim to provide an understanding of their position time series, changes in position, and their behavior in the context of glacier melting, and to evaluate their suitability for further scientific investigations.

6.1. Time series analysis

6.1.1. Nyales20 time series analysis

The investigation began by carefully examining the position time series data for the Nyales20 and Nyale13s radio telescopes. Furthermore, the GNSS timeseries of the NYA2 station was included in the analysis.

These timeseries hold the key to understanding the stability and movements of these stations over study period. This section presents detailed plots and data visualizations, specifically focusing on the X, Y, and Z components of position.

Figure 6.1. presents the absolute position for the Nyales20 station over the study period, accompanied by a simple linear regression line that represent velocities. The precision in the positional data has standard deviations of 14.77 mm and 14.46 mm on the X and Z axes, respectively, whereas the Y axis is more precise, exhibiting a lower standard deviation of 7.49 mm.

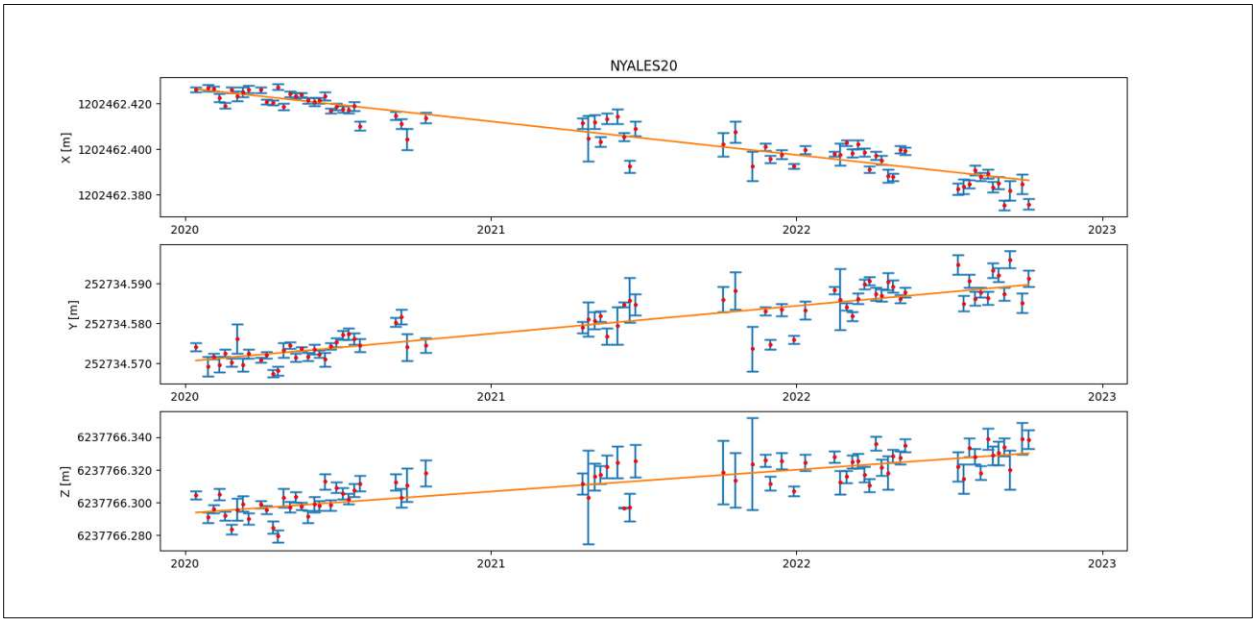

Figure 6.1. Nyales20 absolute position timeseries.

Table 6.1. presents a statistical overview for the Nyales20 station during the study period, including the mean coordinates, weighted mean coordinates, and standard deviations.

NY	mean coordinates (m):	weighted mean coordinates (m):	Standard deviation (mm):
X	1202462.406	1202462.403	X(mm): 14.77
Y	252734.580	252734.581	Y(mm): 7.49
Z	6237766.312	6237766.315	Z(mm): 14.46

Table 6.1. Statistical overview for Nyales20.

Figure 6.2, one can observe the differences in a priori coordinates from ITRF2020 in each axis of the Cartesian coordinates of the Nyales20 antenna during the study period. Notably, minimal biases were found on the X and Y axes, with mean formal errors of 2.21mm and 1.84 mm, weighted means of 1.75 mm and - 2.77 mm, and standard deviations of 4.72 mm and 3.39 mm. Conversely, the height component exhibited larger values, with a mean formal error of approximately 6.1 mm, a weighted mean of 16.48 mm, and a standard deviation of 8.21 mm (see Table 6.2).

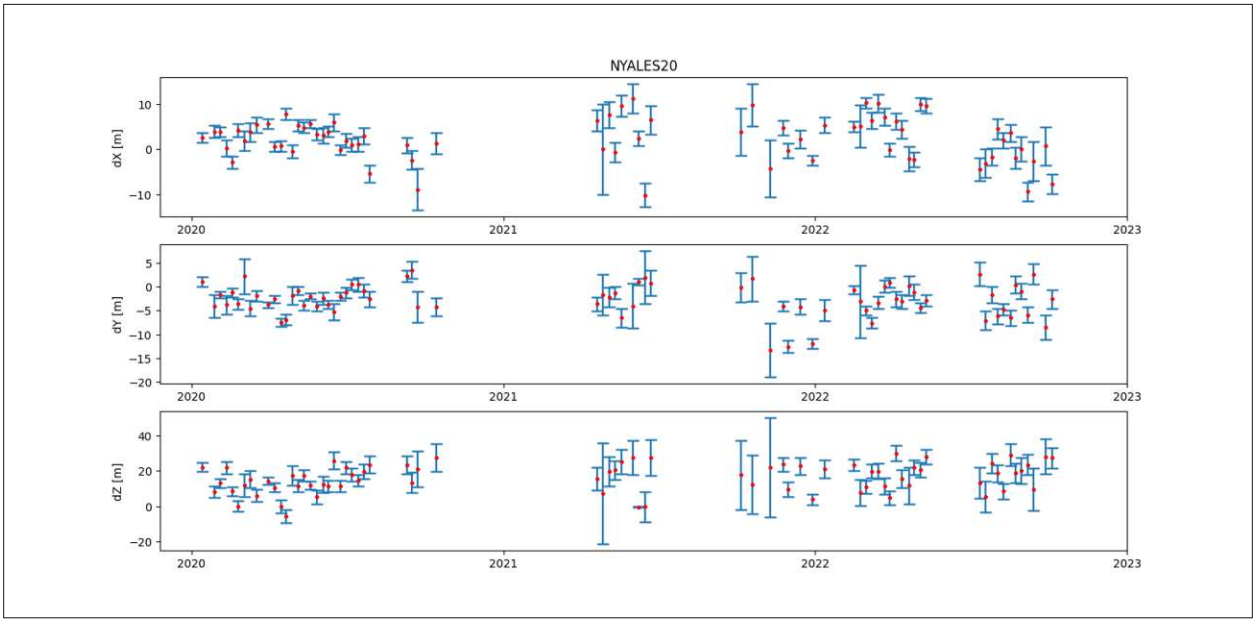

Figure 6.2. Estimated cartesian coordinates with their formal error w.r.t. ITRF2020 for Nyales20.

Table 6.2 exhibits a statistical overview for Nyales20, namely mean formal errors, weighted means, and standard deviation:

NY	Mean formal error	*weighted mean:*	Standard deviation
X(mm)	2.21	*1.75*	4.72
Y(mm)	1.84	*-2.77*	3.39
Z(mm)	6.08	*16.48*	8.21

Table 6.2. Statistical overview for Nyales20 w.r.t. ITRF2020.

Figure 6.3 displays the same results but in local coordinates, specifically dN, dE, and dH.

Minimal biases were found along the dN and dE axes, with mean formal errors of 2.34 mm and 1.85 mm, weighted means of 2.04 mm and - 3.06 mm, and standard deviations of 4.67 mm and 3.52 mm. Conversely, the height component exhibited larger values, with a mean formal error of 5.93 mm, a weighted mean 16.35 mm and, a standard deviation of 8.18 mm (see Table 6.3).

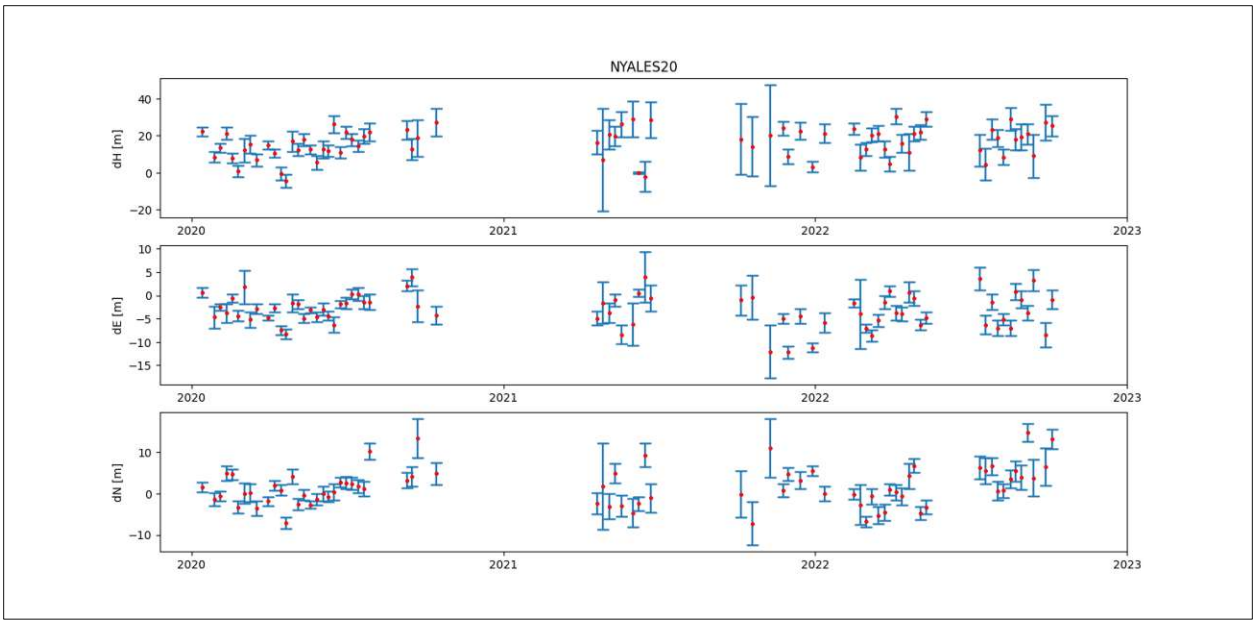

Figure 6.3. Estimated coordinates with respect to ITRF2020 in local system for Nyales20.

Table 6.3 displays a statistical overview for Nyales20, namely mean formal errors, weighted means, and standard deviation:

NY	Mean formal error:	weighted mean:	Standard deviation:
dH(mm)	5.93	16.35	8.18
dE(mm)	1.85	-3.06	3.52
dN(mm)	2.34	2.04	4.67

Table 6.3. Statistical overview for Nyales20 w.r.t. ITRF2020 in local system.

6.1.2. Nyale13s time series analysis

The position time series analysis was extended to the Nyale13s radio telescope, and the following results were observed:

Figure 6.4 depicts the absolute position for Nyale13s between January 2020 and October 2022. The precision in the positional data had standard deviations of 11.50 mm and 18.74 mm on the X and Z axes, respectively. By contrast, the Y axis was more precise, exhibiting a lower standard deviation of 5.72mm.

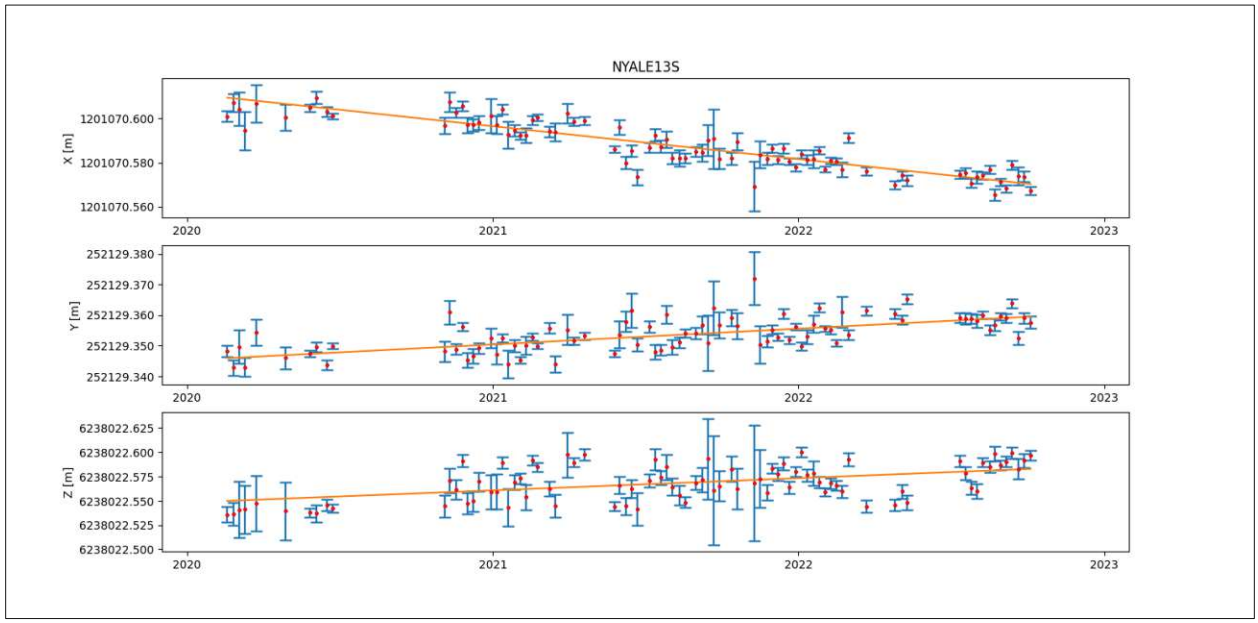

Figure 6.4. Nyale13s absolute position timeseries.

Table 6.4. presents a statistical overview for the Nyale13s station during the study period, including the mean coordinates, weighted mean coordinates, and standard deviations.

NS	mean coord. (m):	weighted mean coord:	Standard deviation (mm):
X	1201070.588	1201070.589	11.50
Y	252129.354	252129.354	5.72
Z	6238022.568	6238022.565	18.74

Table 6.4. Statistical overview for Nyale13s.

Figure 6.5 reveals the position differences with respect to a priori coordinates from ITRF2020 in each axis of the Cartesian coordinates of Nyale13s antenna during the study period.

Minimal biases were found on the X and Y axes, with mean formal errors of 3.21 mm and 2.49 mm, weighted means of - 1.44 mm and - 0.75 mm, and standard deviations of 5.27 mm and 4.39 mm. Conversely, the height component exhibited larger values, with a mean formal error approximately 11.33mm, weighted mean of 6.49 mm and standard deviation of 15.94 mm (see Table 6.5).

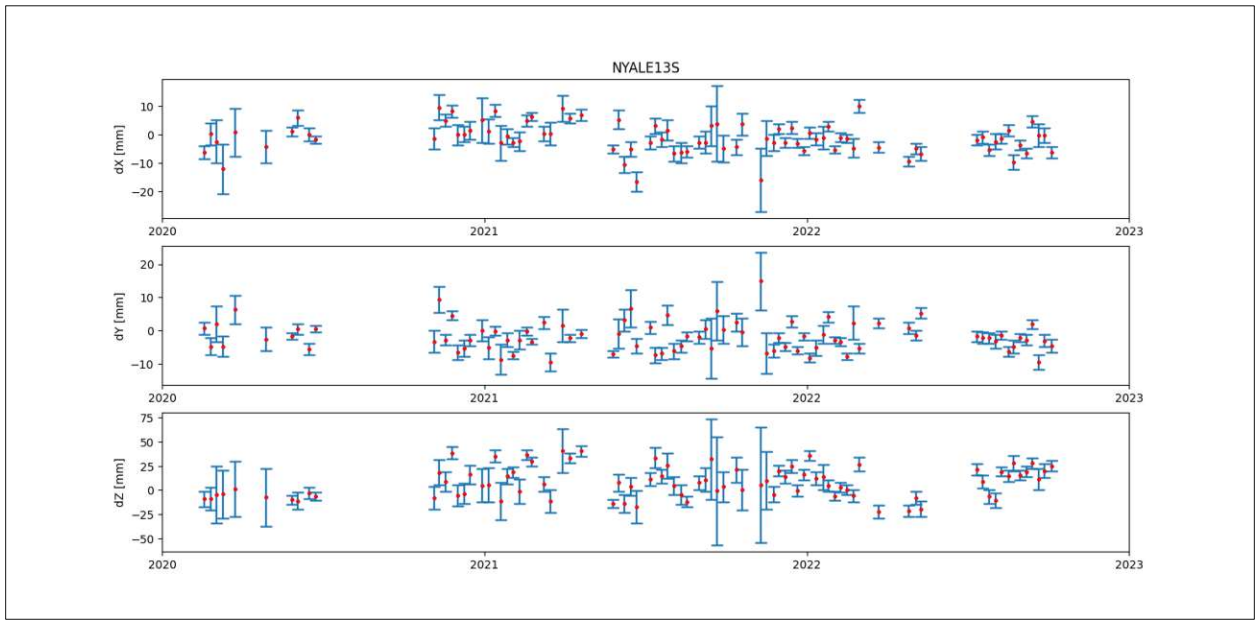

Figure 6.5. Estimated cartesian coordinates with their formal error w.r.t. ITRF2020 for Nyale13s.

Table 6.5 exhibits a statistical overview for Nyale13s, namely mean formal errors, weighted means, and standard deviation:

NS	Mean formal error:	Weighted mean:	Standard deviation:
X	3.21	-1.44	5.27
Y	2.49	-0.75	4.39
Z	11.33	6.49	15.94

Table 6.5. Statistical overview for Nyale13s w.r.t. ITRF2020.

Figure 6.6 illustrates the position differences of the Nyale13s station in local coordinates (dN, dE and DH). Minimal biases were found on the dN and dE axes, with mean formal errors of 3.48 mm and 2.52 mm, weighted means of 2.78 mm and - 0.47 mm, and standard deviations of 4.39 mm and 4.42mm. Conversley, the height component (dH) exhibited larger values, with a mean formal error of 11.02 mm, weighted mean of 6.02 mm and standard deviation of 16.19 mm (see Table 6.6).

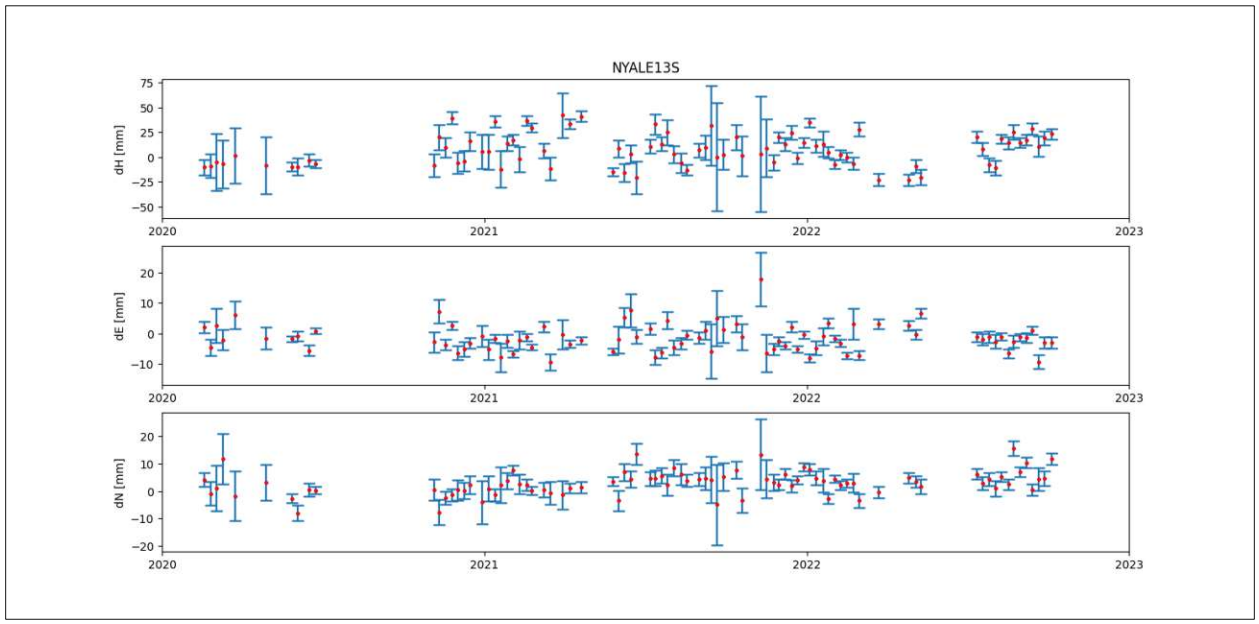

Figure 6.6. Estimated local coordinates with their formal error w.r.t. ITRF2020 for Nyale13s.

Table 6.6 gives a statistical overview for Nyale13s, namely mean formal errors, weighted means, and standard deviation:

NS	Mean formal error:	weighted mean:	Standard deviation:
dH(mm)	11.02	6.02	16.19
dE(mm)	2.52	-0.47	4.42
dN(mm)	3.48	2.78	4.39

Table 6.6. Statistical overview for Nyale13s w.r.t. ITRF2020 in local system.

6.1.3. GNSS-NYA2 Time Series Analysis

Figure 6.7 presents the GNSS time series with respect to the first session of the NYA2 station. The NYA2 GNSS antenna is situated in the region of the Ny-Alesund Observatory, and the dataset was used to compare the results of the VLBI telescopes (Nyales20 and Nyale13s) with those GNSS station NYA2.

Figure 6.7 indicates, the highest bias value was also observed in GNSS measurements in the Z-component with a mean formal error of 4.48 mm and, standard deviation of 10.88 mm.

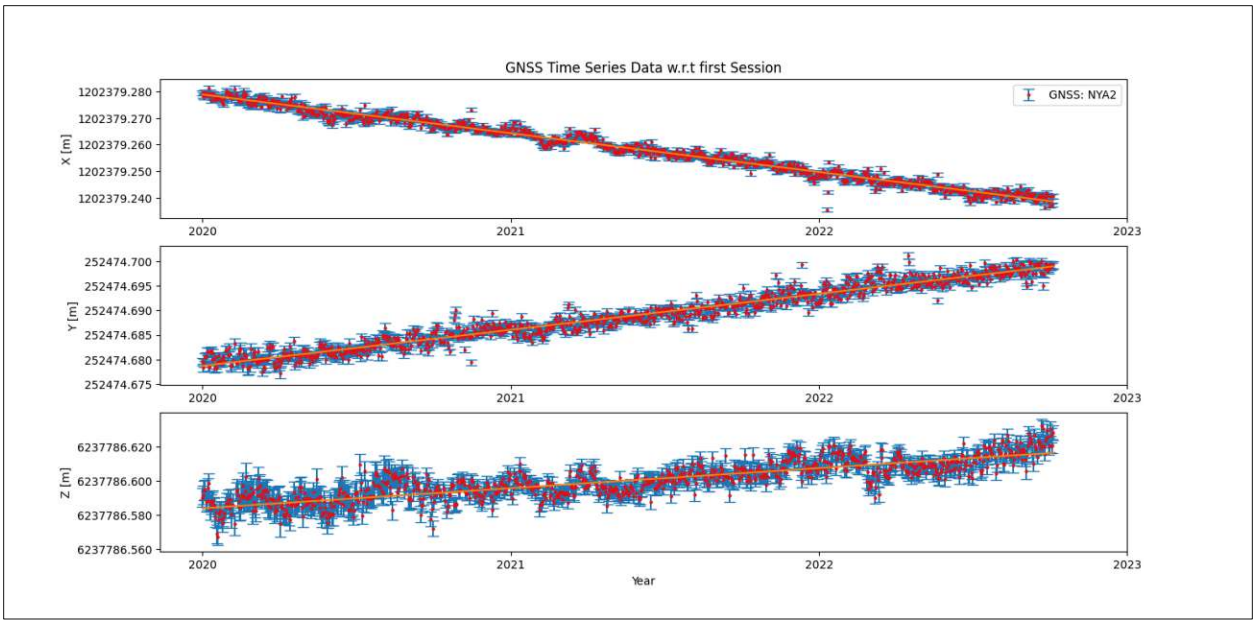

Figure 6.7. GNSS time series of NYA2 antenna.

Table 6.7 presents a statistical overview for the GNSS-NYA2 station during the study period, including the mean coordinates, weighted mean coordinates, mean formal errors, and standard deviations:

NYA2	Mean coordiantes (m):	Weighted mean coordinates (m):	Mean formal error (mm):	Standard deviation (mm):
X	1202379.259	1202379.260	0.85	11.68
Y	252474.689	252474.688	0.69	5.99
Z	6237786.600	6237786.599	4.48	10.88

Table 6.7. Statistical overview for NYA2.

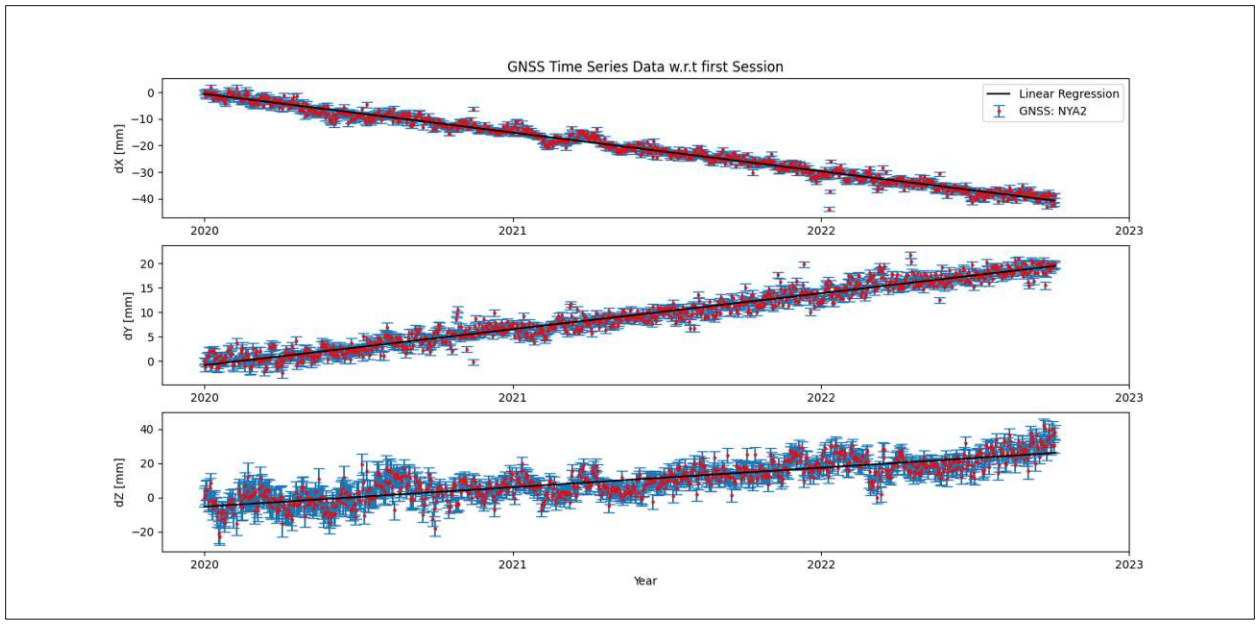

Figure 6.8. GNSS time series of the NYA2 antenna w.r.t. 1st session.

6.2. Position changes assessment (Uplift comparison with o-located GNSS antenna)

In this phase of our analysis, we focus on determining whether the positional changes of the Nyales20, Nyale13s and NYA2 antennas demonstrated agreement. Additionally, we analysed any significant changes in height, and speculated on whether they can be attributed to glacier melting.

To quantify the observed position changes, we utilized velocity estimations determined through a linear regression of session-wise estimated station coordinates.

The velocities for the VLBI stations Nyales20 and Nyale13s, as well as the GNSS site NYA2, are as follows:

- *NY: [vx, vy, vz]: [-14.6, 7.0, 13.3] mm/year*
- *NS: [vx, vy, vz]: [-15.0, 5.2, 12.6] mm/year*
- *NYA2: [vx, vy, vz]: [-14.59, 7.36, 11.76] mm/year*

To offer context and facilitate comparisons, we present our results alongside the ITRF2020 velocities:

- *ITRF 2020 velocities for NY: [vx, vy, vz]: [-14.5, 7.6, 10.6] mm/year*
- *ITRF 2020 velocities for NS: [vx, vy, vz]: [-12.8, 5.6, 10.2] mm/year*

Additionally, Nyales20 participated in 292 sessions, whereas Nyale13s participated in 336 sessions. Furthermore, parallel sessions between these two telescopes were calculated, resulting in 77 parallel sessions during the almost three-years study period.

6.2.1. Position change between Nyales20 and Nyale13s

Figure 6.9 displays the position changes relative to the first session between Nyales20 and Nyale13s in a shared plot. The results indicated minimal changes in velocity for Nyales20 compared with ITRF2020 in the X and Y axes exhibited a good agreement, respectively Δvx = - 0.1 mm/year and Δvy = 0.6 mm/year, while the height component indicated a change of Δvz = 2.7 mm/year.

By contrast, Nyale13s exhibited significant discrepancies in the X and Z components (Δvx = -2.2 mm/year and Δvz = 2.4 mm/year), with good agreement in the Y component (Δvy = - 0.4mm/year).

Finally, the changes in the Nyales20 and Nyale13s antennas relative to each other were as following:

*Ny-Ns: [vx, vy, vx] = [-0.4, 1.8, 0.7] mm/year, indicating higher discrepancies on the Y and Z axes (*Δvy = 1.8mm/year and Δvz = 0.7mm/year).

Based on the results, specifically velocity values gained after our analysis and taking into account the number of parallel sessions between these two stations, we concluded that the changes were minor; therefore, the transfer of the velocities from the old system to the new one can be achieved after 3 years of parallel running. This helped us to achieve one of our study objectives.

Since, the observatory's location in the Arctic, in the region of several large glaciers, according to (Garcia-Espada et al., 2022) has been confirmed that Svalbard's glaciers are losing mass due to climate change, which influences the stability of the reference frames.

Furthermore, height biases were detected in the VLBI and GNSS time series data, this provided support for geophysical processes such as glacier melting being potential contributing factors.

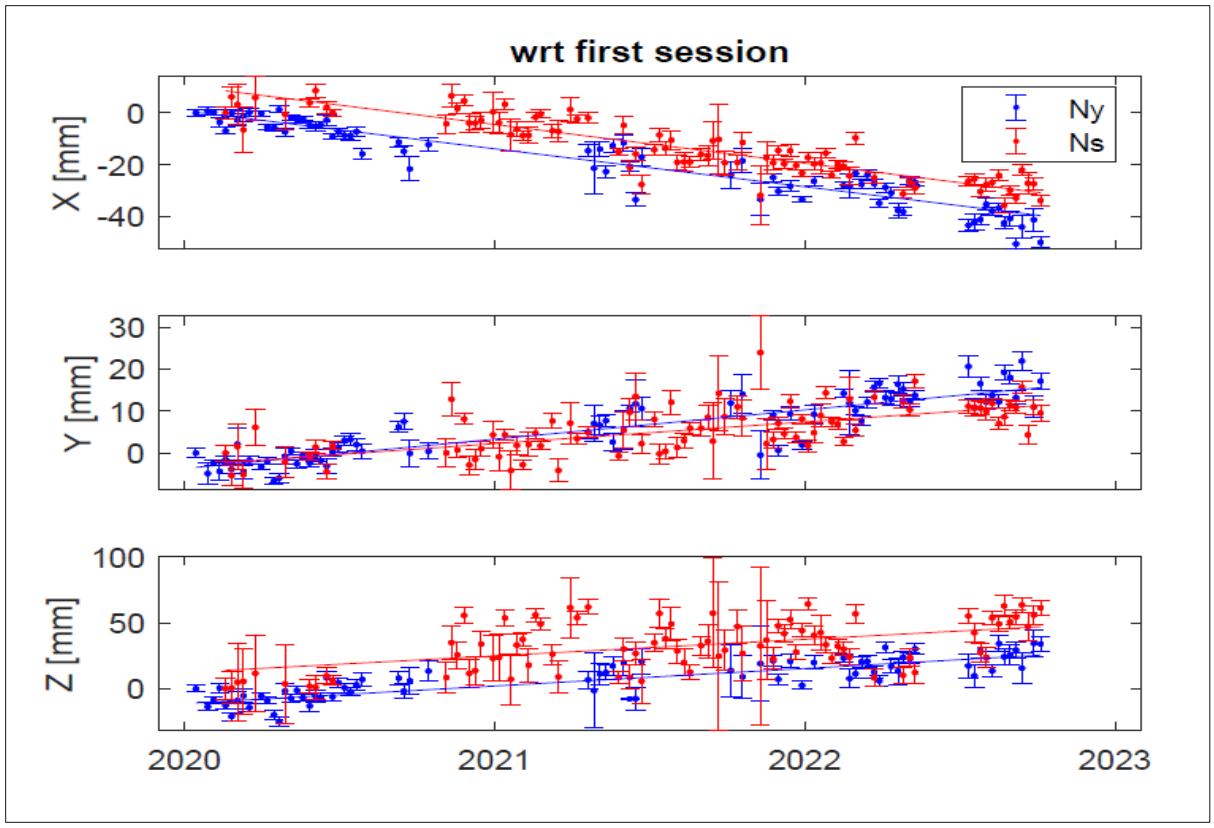

Figure 6.9. Comparison between Nyales20 and Nyale13s time series w.r.t. first session.

6.2.2. Position change between Nyales20 and NYA2

Another objective of this study was to compare the time series of two different space-geodetic techniques, specifically VLBI and GNSS. This comparative analysis offered valuable insights into the alignment and discrepancies between the time series of Nyales20 and Nyale13s on the one hand and the GNSS time series of the NYA2 antenna on the other hand.

Figure 6.10 illustrates the positional variance between Nyales20 and the GNSS antenna NYA2. The shared plot reveals a clear alignment between these two sets of measurements. The differences were minimal along X and Y axes (Δvx = 0.01 mm/year and Δvy = -0.36mm/year). Higher discrepancies were found on the Z axis (Δvz = 1.54mm/year).

- *NY: [vx, vy, vz]: [-14.6, 7.0, 13.3] mm/year*
- *NYA2: [vx, vy, vz]: [-14.59, 7.36, 11.76] mm/year*

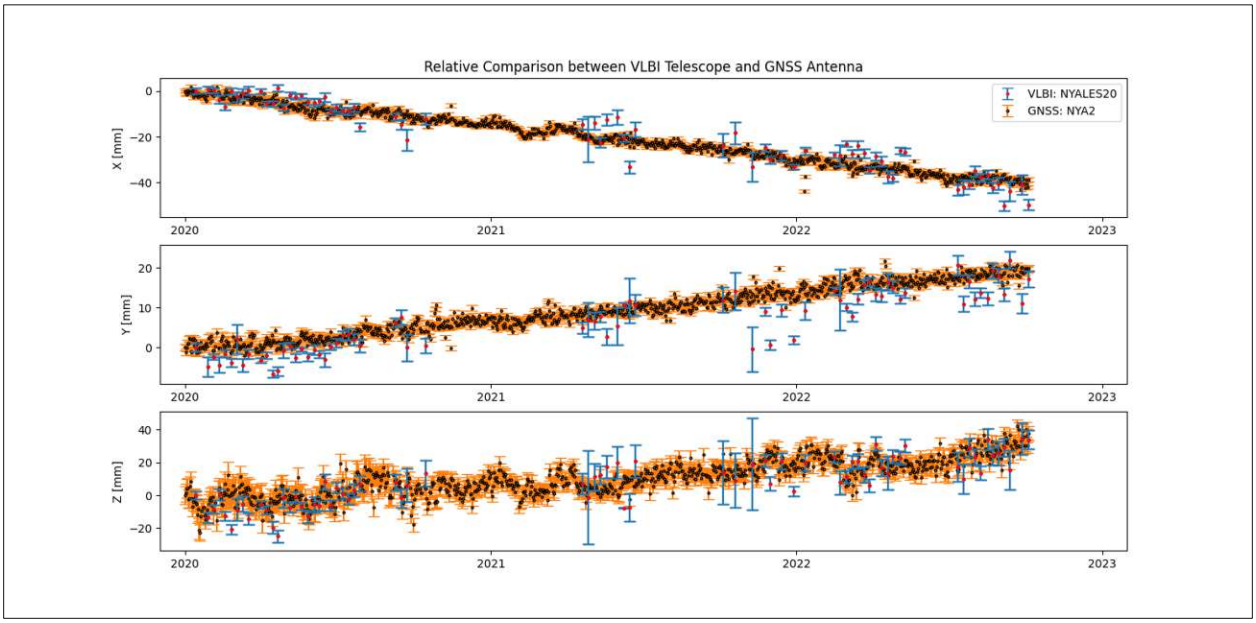

Figure 6.10. Relative comparison between VLBI (Nyales20) and GNSS (NYA2) time series.

6.2.3. Position change between Nyale13S and NYA2

By contrast, Figure 6.11 presents a comparison between the VLBI station Nyale13s and the GNSS station NYA2. The changes were predominantly observed on Y and Z axes with Δvy = - 2.16 mm/year and Δvz = 0.84 mm/year, indicating considerable variations. On the other hand, the changes on the X axis (Δvx = 0.41mm/year) appeared to be smaller.

- *NS: [vx, vy, vz]: [-15.0, 5.2, 12.6] mm/year*
- *NYA2: [vx, vy, vz]: [-14.59, 7.36, 11.76] mm/year*

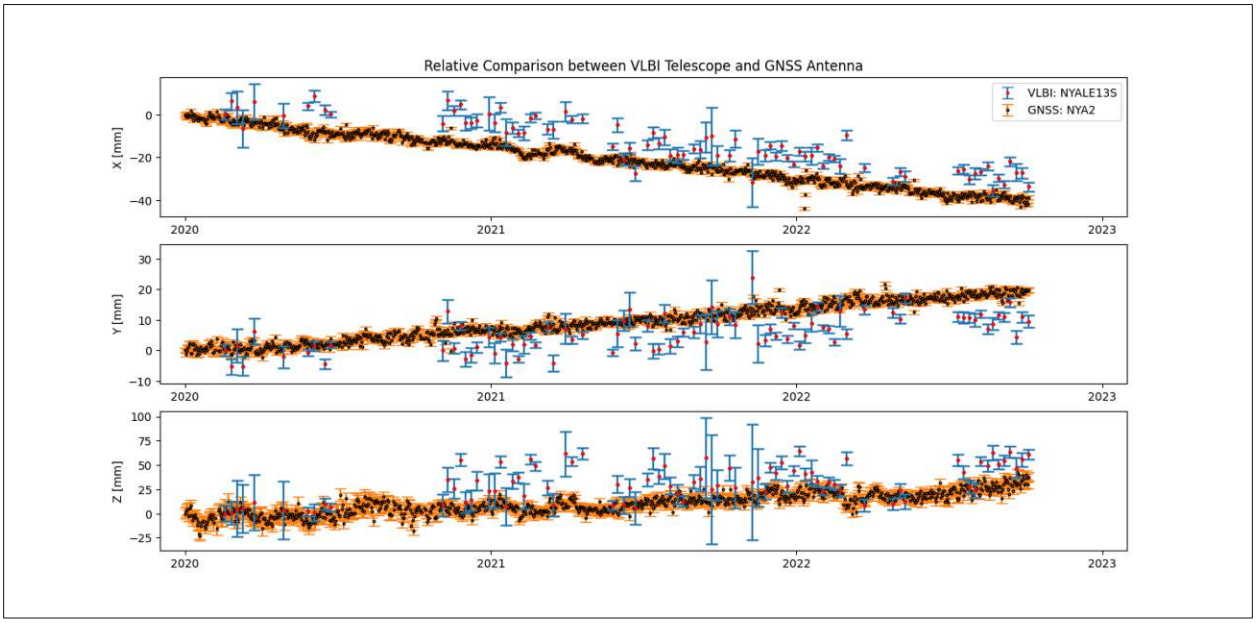

Figure 6.11. Relative comparison between VLBI (Nyale13s) and GNSS (NYA2) time series.

6.2.4. Baseline repeatability

Additionally, Figure 6.12 illustrates the position changes between the stations Nyales20 and Nyale13s, providing insights into baseline shifts. The estimated baseline length, with respect to the first session value (1539.1932m), exhibited a mean formal error of 2.18 mm over the study period, accompanied by a weighted mean weighted mean of 0.88mm and a standard deviation of 4.08 mm.

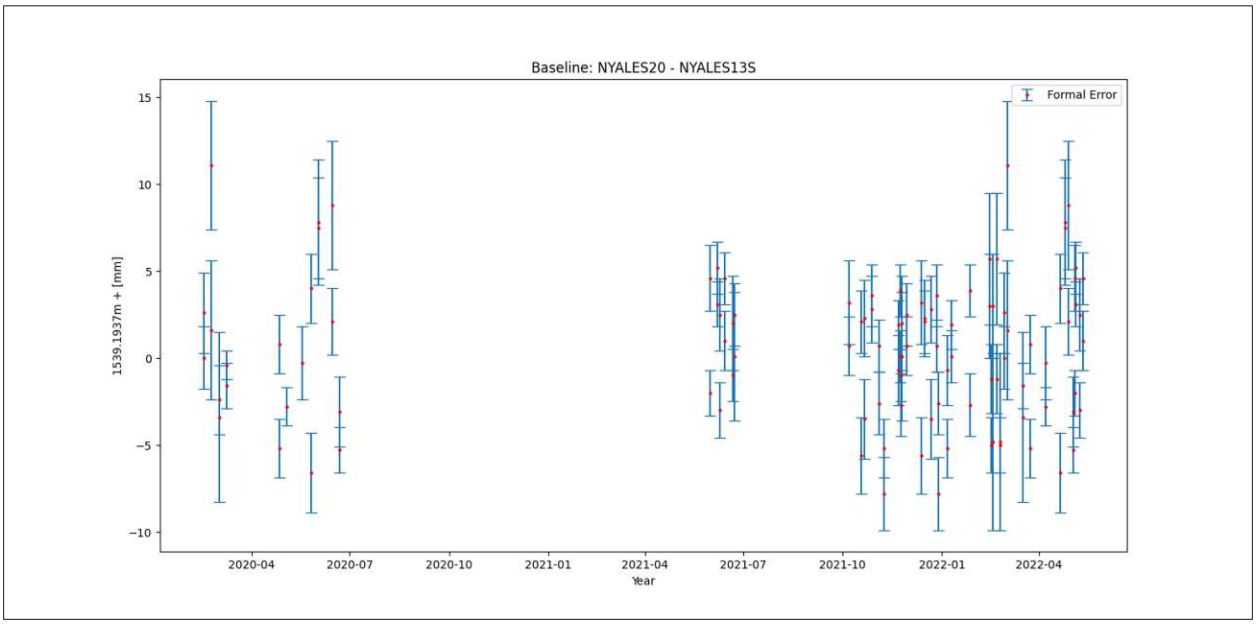

Figure 6.12. Estimated baseline length with formal error with respect to the 1st session.

6.3 Impact of Nyales20 and Nyale13s on EOP

This section presents the results of an analysis of multiple VLBI sessions, incorporating various ground stations. It aimed to evaluate the impact of including or excluding specific VLBI telescopes, namely Nyales20 and Nyale13s, on the precision and repeatability of the estimated EOP. The study's objective was to determine whether the timespan of the legacy telescope Nyales20 should be prolonged based on the results obtained from these sessions.

Two VLBI sessions were used for this analysis, namely R1-1027 and R4-1033. Additionally, VieSched++ (see Section 4.3) enabled us to perform the sessions and deal with this study objective.

6.3.1 Workflow in VieSched++

The purpose of using VieSched++ was to create schedules and simulate the results for two different sessions, namely R1-1027 and R4-1033. For each session, three different schedules were generated one with all stations participating, one excluding Nyales20 and finally one by excluding both Nyales20 and Nyale13s. These schedules were subjected to 1000 simulations, which provided estimated values such as mean formal errors and repeatability.

These estimated values served to address the following objectives of this study:

- To evaluate whether the performance of the sessions improved with or without Nyales20 and Nyale13s, thus determining the impact of these two stations;
- To determine whether the operational life of the old station Nyales20 should be extended;
- To evaluate whether, in the absence of Nyales20 observation, the station Nyale13s can continue to observe in the S/X band or whether an upgrade to the new-generation VGOS is necessary.

Tables 6.8 and 6.9 describe the parametrization of the schedules and simulations performed for this case study:

IVS R11027	
Start	29.11.2021 (17:00)
Duration	24h
Observing mode:	512-16 (CONT11)
Sources:	Source.cat.geodetic.good
DOWNTIME:	WZ 2021-333-18:15:00 2021-333-19:45:00
Weighted Station:	AGGO 2.00
Simulation for all stations:	clock ASD: 10^-14 s, tropo Cn: 1.8*10^-7 m^-1/3, white noise: 17.68 ps
Simulation runs:	1000x
IVS-R11027 was scheduled	All stations, Without NYALES20 Without NYALES20 & NAYLE13S

Table 6.8. Scheduling/simulation parameters for the IVS R1-1027 session.

IVS R41033	
Start	13.01.2022 (18:30)
Duration	24h
Observing mode:	512-16 (CONT11)
Sources:	Source.cat.geodetic.good
DOWNTIME:	WZ 2022-13-18:30:00 2022-13-19:45:00
Weighted Station:	HART15M 2.00
Simlation for all stations:	clock ASD: 10^-14 s, tropo Cn: 1.8*10^-7 m^-1/3, white noise: 17.68 ps
Simulation runs:	1000x
IVS-R41033 was scheduled	All stations, Without NYALES20 Without NYALES20 & NAYLE13S

Table 6.9. Scheduling/simulation parameters for the IVS R4-1033 session.

These simulations were carried out as standard S/X observations based on:

- Tropo Cn – Tropospheric Refractive Index Structure Parameter – is used to model the impact of the Earth's troposphere on the signal propagation (Böhm, J., & Schuh, H. 2013);
- Clock ASD – Allan Standard Deviation – is used to characterize the stability of clocks (https://home.engineering.iastate.edu - Allan variance).
- White noise – is associated with the system noise or errors in measurements (Schartner, M. et.al., 2018).

6.3.2. Session 1: IVS R1-1027

This session, coded as IVS-R1, took place on November 29, 2021, for a full 24 hours of observation. It involved a network of 16 stations. NASA, the operations center, successfully managed this session, and the collected data were correlated using the BONN correlator. The data from this session have been released and analyzed by NASA (*IVS web site*).

With all stations participating:

In the initial configuration with all stations participating, the mean formal error values for the key parameters, namely XPO and YPO, were 15.02 µas and 17.87 µas. Additionally, dUT1, NUTX, and NUTY had mean formal error values of 0.9670 mus, 11.02, and 10.89 µas, respectively.

The repeatability values were 30.82 µas (XPO), 34.95 µas (YPO), 2.0449 µs (dUT1), 22.66 µas (NUTX), and 22.46 µas (NUTY).

Figure 6.13 displays a map of the stations network that participated in session IVS R1-1027:

| AGGO |HART15M | ISHIOKA | KOKEE |MATERA | NOTO | NYALE13S| NYALES20 | ONSALA60 |
| RAEGSMAR | SEJONG | SESHAN25 | WARK12M | WETTZELL |YARRA12M | YEBES40M |

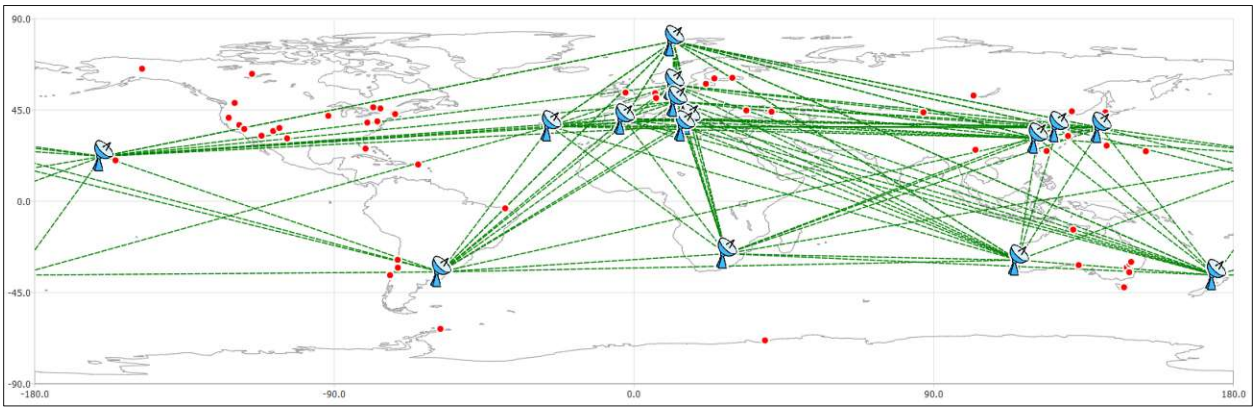

Figure 6.13. Map of the stations that participated in session IVS R1-1027.

Table 6.10 presents the mean formal errors and repeatability values in session R11027

Mean formal errors: R1-1027

v	score	#obs	XPO	YPO	dUT1	NUTX	NUTY
	[]	[]	[muas]	[muas]	[mus]	[muas]	[muas]
0	0.0000	19060	15.0216	17.8730	0.9670	11.0233	10.8916

Repeatability: R1-1027

v	score	#obs	XPO	YPO	dUT1	NUTX	NUTY
	[]	[]	[muas]	[muas]	[mus]	[muas]	[muas]
0	0.0000	19060	30.8161	34.9457	2.0449	22.6607	22.4645

Table 6.10. Impact of including all stations in session R11027.

Excluding NYALES20:

Excluding Nyales20 station from the initial configuration led to changes in formal error and repeatability values for key Earth Orientation Parameters. The formal error values for XPO and YPO increased by approximately 4.20%, indicating a slight decrease in accuracy. The formal error for Dut1 increased by 14.86%, while NUTX and NUTY experienced changes of approximately 2.27% and 9.27% respectively.

The repeatability values demonstrated varying trends. The repeatability of XPO slightly decreased by - 2.62%, while YPO decreased by 4.91%. Conversely, Dut1's repeatability increased by 3.79%, and NUTX and NUTY exhibited decreases of approximately - 5.57% and - 1.96%, respectively (see Table 6.12).

| AGGO | HART15M | ISHIOKA | KOKEE | MATERA | NOTO | NYALE13S | ~~**NYALES20**~~|
|ONSALA60|RAEGSMAR | SEJONG |SESHAN25 | WARK12M | WETTZELL | YARRA12M |
|YEBES40M |

Mean formal errors: R1-1027

v	score	#obs	XPO	YPO	dUT1	NUTX	NUTY
	[]	[]	[muas]	[muas]	[mus]	[muas]	[muas]
0	0.0000	16235	15.6544	18.6166	1.1111	11.2733	11.8960

Repeatability: R1-1027

v	score	#obs	XPO	YPO	dUT1	NUTX	NUTY
	[]	[]	[muas]	[muas]	[mus]	[muas]	[muas]
0	0.0000	16235	30.0095	33.2252	2.1223	21.4048	22.0222

Table 6.11. Impact of excluding Nyales20 from session R11027.

Excluding Ny	XPO	YPO	Dut1	NUTX	NUTY
Mean formal error (%)	+4	+4	+15	+2	+9
Repeatability (%)	-2.5	-5	+4	-5	-2

Table 6.12. Percentage impact of excluding Nyales20 from session R11027.

Excluding NYALES20 and NYALE13S:

Upon excluding both stations, a slight increase in mean formal error values was observed (see Table 6.12). Specifically, XPO increased by approximately +3.06%, indicating a decrease in accuracy, while YPO decreased by approximately -1.4%. Moreover, Dut1, NUTX, and NUTY had mean formal error values that increased by approximately +22.94%, 3.81% and 6.8%, respectively.

The repeatability values also decreased, with XPO (- 4.7 %), and YPO (- 11%). Additionally, NUTX and NUTY had repeatability values that decreased by approximately - 3%, and - 3.8%, respectively., whereas DUT1 increased by 8.7% (see Table 6.14).

Figure 6.14 shows a map of the stations network in session IVS R1-1027, after exclusion of Nyales20 and Nyale13s:
| AGGO | HART15M | ISHIOKA | KOKEE | MATERA | NOTO | ~~**NYALE13S**~~ | ~~**NYALES20**~~|
|ONSALA60| RAEGSMAR | SEJONG | SESHAN25 | WARK12M | WETTZELL | YARRA12M |
|YEBES40M |

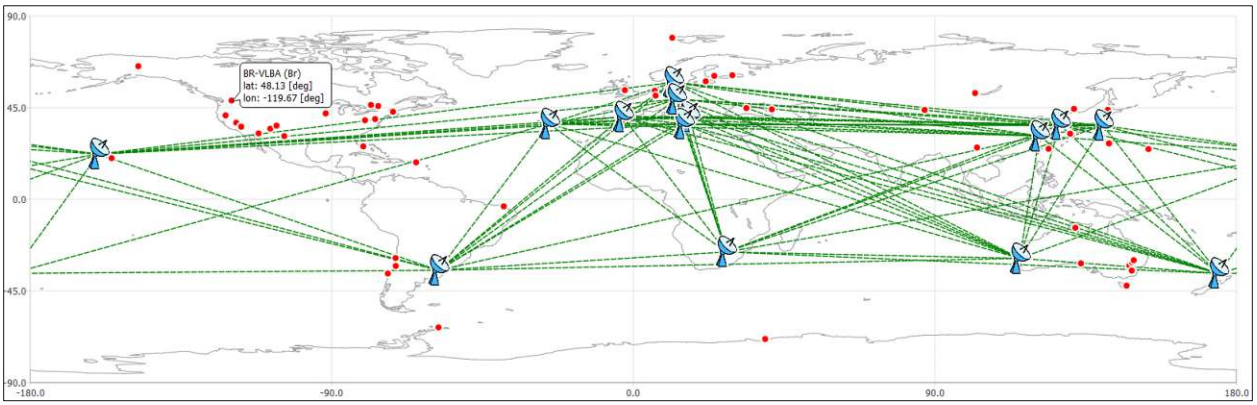

Figure 6.14. Map stations that participated in session IVS R1-1027 (excluding Ny and Ns).

Mean formal errors: R1-1027

v	score	#obs	XPO	YPO	dUT1	NUTX	NUTY
	[]	[]	[muas]	[muas]	[mus]	[muas]	[muas]
0	0.0000	14751	15.4763	17.6187	1.1886	11.4356	11.6317

Repeatability: R1-1027

v	score	#obs	XPO	YPO	dUT1	NUTX	NUTY
	[]	[]	[muas]	[muas]	[mus]	[muas]	[muas]
0	0.0000	14751	31.1727	32.4646	2.4694	21.9915	21.5883

Table 6.13. Impact of excluding both Nyales20 and Nyale13s from session R11027.

Excluding Ny&Ns	XPO	YPO	Dut1	NUTX	NUTY
Mean formal error (%)	+3	-1.5	+22	+4	+7
Repeatability (%)	+1	-7	+20	-3	-4

Table 6.14. Percentage impact of excluding Nyales20 and Nyale13s from session R11027.

6.3.3 Session 2: IVS R4-1033

This session began on January 13, 2022, at 18:30, for a full 24 hours of observation mode. Data were gathered from the following 11 stations: Ht, Is, Kk, Ns, Ny, Sa, Ww, Wz, Yg, Ys, and Zc. The USNO managed this session, and data processing was executed using the WASH correlator. The session's data were successfully released and subsequently analysed by USNO (*IVS web site*).

All stations participating:

In the initial configuration with all stations participating, the mean formal error values for the key parameters, namely XPO and YPO, were 18.48 µas and 24.03 µas. Additionally, dUT1, NUTX, and NUTY had mean formal error values of 1.1788 µs, 12.05 µas, and 11.80 µas, respectively.

The repeatability values were 36.06 µas (XPO), 47.58 µas (YPO), 2.3945 µs (dUT1), 22.08 µas (NUTX), and 21.96 µas (NUTY)

Figure 6.15 displays a map of the stations network that participated in session IVS R4-1033:

| HART15M | ISHIOKA | KOKEE | NYALE13S | NYALES20 | RAEGSMAR | WARK12M | WETTZELL|
| YEBES40M|YARRA12M | ZELENCHK |

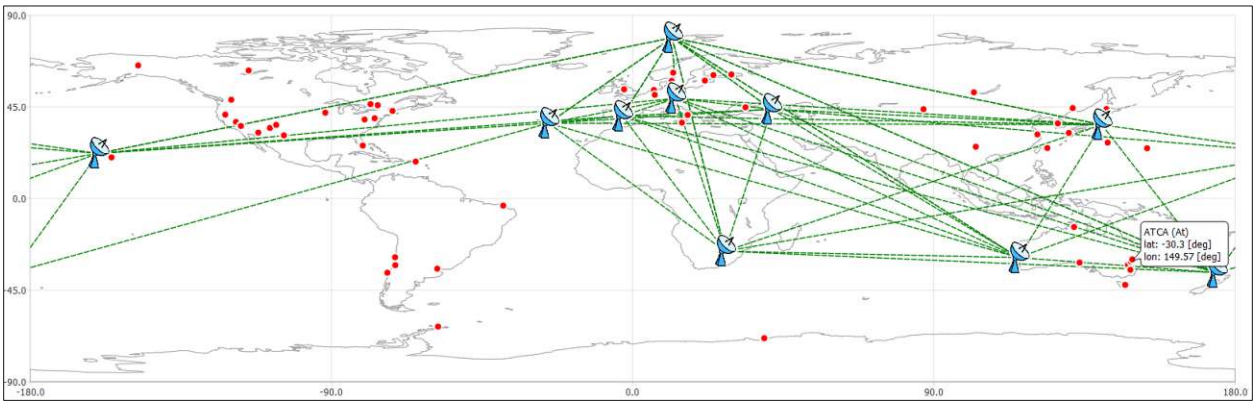

Figure 6.15 Map of stations that participated in session IVS R4-1033.

Mean formal errors: R4-1033

v	score	#obs	XPO	YPO	dUT1	NUTX	NUTY
	[]	[]	[muas]	[muas]	[mus]	[muas]	[muas]
0	0.0000	12772	18.4818	24.0257	1.1788	12.0531	11.7957

Repeatability: R4-1033

v	score	#obs	XPO	YPO	dUT1	NUTX	NUTY
	[]	[]	[muas]	[muas]	[mus]	[muas]	[muas]
0	0.0000	12772	36.0648	47.5766	2.3945	22.0767	21.9596

Table 6.15 Impact of including all stations in session R41033.

Excluding NYALES20:

In the comparison between the initial configuration that involved all stations and the scenario that excluded Nyales20, distinctive variations were observed in mean formal error values alongside their corresponding repeatability measurements for key parameters.

For XPO, a reduction of approximately 3.78% in mean formal error was noted, accompanied by a 3.07% decrease in repeatability. Conversely, YPO exhibited an increase of approximately 4.36% in mean formal error, coupled with a more substantial -6.8% decrease in repeatability.

Furthermore, the parameter Dut1 exhibited a significant 10.48% increase in mean formal error, with a marginal 0.51% rise in repeatability; NUTX exhibited a 5.54% increase in mean formal error alongside an 8.54% growth in repeatability; and lastly NUTY exhibited a 7 % increase in mean formal error, while the repeatability exhibited a more pronounced rise of 11% (see *Table 6.17*).

| HART15M | ISHIOKA | KOKEE | NYALE13S | ~~**NYALES20**~~ | RAEGSMAR | WARK12M | WETTZELL | YEBES40M |YARRA12M | |ZELENCHK |

Mean formal errors: R4-1033

v	score	#obs	XPO	YPO	dUT1	NUTX	NUTY
	[]	[]	[muas]	[muas]	[mus]	[muas]	[muas]
0	0.0000	10106	17.7933	25.0731	1.3035	12.7102	12.6438

Repeatability: R4-1033

v	score	#obs	XPO	YPO	dUT1	NUTX	NUTY
	[]	[]	[muas]	[muas]	[mus]	[muas]	[muas]
0	0.0000	10106	34.8655	44.3278	2.4081	23.9088	24.4797

Table 6.16. Impact of excluding Nyales20 from session R41033.

Excluding Ny	XPO	YPO	Dut1	NUTX	NUTY
Mean formal error (%)	-3	+4	+10	+5.5	+7
Repeatability (%)	-3	-7	+0.5	+8	+11

Table 6.17. Percentage impact of excluding Nyales20 from session R11027.

Excluding NYALES20 and NYALE13S:

Further exclusion of Nyales20 and Nyale13s resulted in an additional increase in mean formal error and repeatability. Notably, XPO decreased by - 2% in mean formal error and approximately 5% in repeatability, while YPO increased by 2.73% in mean formal error and - 11.65% in repeatability. Dut1 exhibited a 15.37% increase in mean formal error, and NUTX and NUTY increased by 9.92% and 14% respectively. Repeatability values for these parameters increased by approximately 8.7% and 6.5% (see *Table 6.18)*.

Figure 6.18 shows a map of the stations network in session IVS R4-1033, after exclusion of Nyales20 and Nyale13s:

| HART15M | ISHIOKA | KOKEE | ~~**NYALE13S**~~ | ~~**NYALES20**~~ | RAEGSMAR | WARK12M |WETTZELL| | YEBES40M | YARRA12M | ZELENCHK |

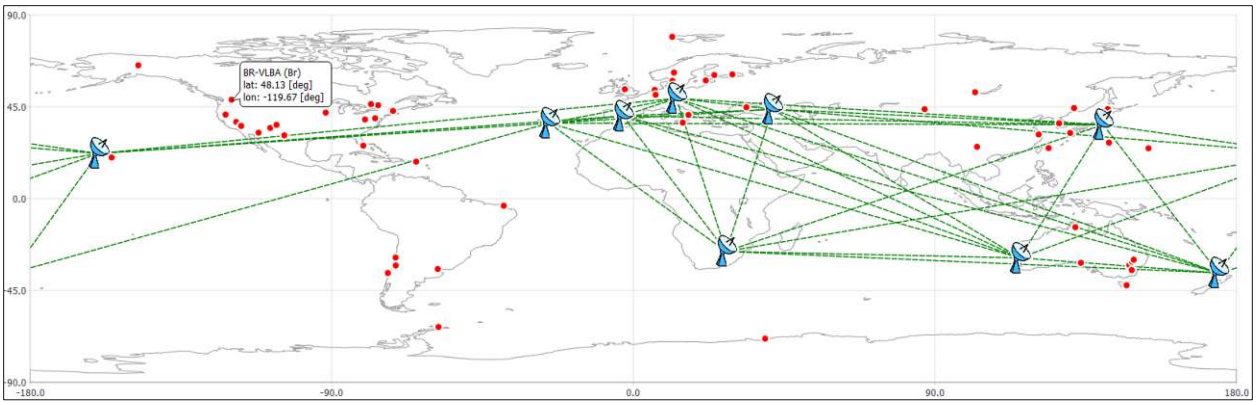

Figure 6.16. Map of stations that participated in session IVS R4-1033 (excluding Ny and Ns).

Mean formal errors: R4-1033

v	score	#obs	XPO	YPO	dUT1	NUTX	NUTY
	[]	[]	[muas]	[muas]	[mus]	[muas]	[muas]
0	0.0000	8417	18.0723	24.6343	1.3589	13.2402	13.4630

Repeatability: R4-1033

v	score	#obs	XPO	YPO	dUT1	NUTX	NUTY
	[]	[]	[muas]	[muas]	[mus]	[muas]	[muas]
0	0.0000	8417	34.3744	42.2421	2.5530	23.9988	23.3742

Table 6.18. Impact of excluding both Nyales20 and Nyale13s from session R41033.

Excluding Ny&Ns	XPO	YPO	Dut1	NUTX	NUTY
Mean formal error (%)	-2	+2.5	+15	+10	+14
Repeatability (%)	-5	-11	+6.5	+9	+6.5

Table 6.18. Percentage impact of excluding Nyales20 and Nyale13s from session R11027.

During these two sessions, the trend was consistent. Excluding the VLBI telescopes Nyales20 and Nyale13s mostly led to an increase in mean formal error values and repeatability values for key the parameters (i.e., XPO, YPO, dUT1, NUTX, and NUTY). These higher values indicated a reduction in accuracy. Therefore, based on the analysis of the results, keeping both Nyales20 and Nyale13s in the observations led to better results and less repeatability, which may affect the accuracy and reliability of the data. The data indicated that sticking to the timespan of the old telescope Nyales20 has a positive impact for maintaining data quality.

However, due to maintenance and economic concerns, Nyales20 was dismantled on August 14, 2023. This decision was influenced by factors such as airport safety, since the antenna was close to the runway of the local airstrip, and the increasing difficulty and expenses of maintaining the antenna due to outdated spare parts (Garcia-Espada et al., 2022).

7. Conclusion

In conclusion, analysis of the time series data obtained from the two northernmost VLBI telescopes, namely Nyales20, Nyale13s, and GNSS-NYA2 site provided valuable results into the dynamics of position changes over the study period.

The velocities and standard deviations calculated for each station offer a nuanced understanding of their respective motions, mainly on X and Z axes, with the Z axis leading.

Velocities:

- *NY: [vx, vy, vz]: [-14.6, 7.0, 13.3] mm/year*
- *NS: [vx, vy, vz]: [-15.0, 5.2, 12.6] mm/year*
- *NYA2: [vx, vy, vz]: [-14.59, 7.36, 11.76] mm/year*

Standard deviation:

- *NY: [vx, vy, vz]: [14.77, 7.49, 14.46] mm*
- *NS: [vx, vy, vz]: [11.0, 5.72, 18.74] mm*
- *NYA2: [vx, vy, vz]: [11.68, 5.99, 10.88] mm*

Additionally, the position change (velocities) during the study period, fits very well to the results of the ITRF2020 for both stations, where the highest bias value w.r.t. ITRF2020 was found in the height component, Δvz = 2.7mm/year (Nyales20) and Δvz = 2.4mm/year, and Δvx = 2.2mm/year for (Nyale13s). The other components corresponded very well to the reference velocities.

On the other hand, the GNSS NYA2 site velocities exhibited discrepancies in the Z component relative to Ny and NS (Δvx =1.54, Δvx =0.84 mm/year). Based on the results, we can state that the changes in the Z-component may be attributed glacier melting.

Moreover, Nyales20 participated in 292 sessions, while Nyale13s participated in 336 sessions throughout the study period. Our analysis of the parallel sessions between these two stations revealed 77 instances of simultaneous operation over the nearly three-year observation period.

Based on the agreement of the position change values (velocities) calculated between both VLBI telescopes and the number of parallel sessions, we can confidently affirm the possibility of transferring velocities from the legacy Nyales20 to the new-generation VGOS telescope Nyale13s.

Finally, to address the impact of the Nyales20 telescope, we employed VieSched++ software (see Chapter 6). The analysis revealed that excluding Nyales20 and Nyale13s led to a notable increase in mean formal errors and repeatability values. This suggests that maintaining both telescopes within the network enhances accuracy. However, assessing the prolonged operation of Nyales20 telescope requires consideration of broader factors beyond accuracy alone. Economic concerns, such as the antenna's proximity to the airstrip and the expensive costs of maintenance due to outdated spare parts, influenced the decision to dismantle Nyales20 on August 14, 2023 (Garcia-Espada et.al., 2022). Despite its positive impact on the quality of the data, the practical implications encourage its cancellation. This underscores the need for an evaluation that balances scientific objectives with logistical and financial realities when making decisions regarding telescope operation.

References

Schuh, H., Böhm, J. (2013). Very Long Baseline Interferometry for Geodesy and Astrometry. In: Xu, G. (eds) Sciences of Geodesy - II. Springer, Berlin, Heidelberg. ttps://doi.org/10.1007/978-3-642-28000-9_7

Guochang Xu. (2013). Editor Sciences of Geodesy - II Innovations and Future Developments. DOI10.1007/978-3-642-28000-9

Hinteregger, H. F., Shapiro, I. I., Robertson, D. S., Knight, C. A., Ergas, R. A., Whitney, A. R., Rogers, A. E. E., Moran, J. M., Clark, T. A., Burke, B. F. (1972). Precision Geodesy via Radio Interferometry. Science, 178: 396-398

Cohen, M. H., Jauncey D .L., Kellerman, K. I., Clark, B. G. (1968). Radio Interferometry at One-Thousandth Second of Arc. Science, Vol. 162: 88-94

Schuh, H., Behrend, D: (2012). VLBI: A fascinating technique for geodesy and astrometry. https://doi.org/10.1016/j.jog.2012.07.007

Schartner, M. (2018). *VieSched++: A new Scheduling Tool in VieVS*.

Schartner, M., & Böhm, J. (2019). VieSched++: A New VLBI Scheduling Software for Geodesy and Astrometry. *Publications of the Astronomical Society of the Pacific*, *131*(1002), 084501. https://doi.org/10.1088/1538-3873/ab1820

Schuh, H., & Behrend, D. (2012). VLBI: A fascinating technique for geodesy and astrometry. *Journal of Geodynamics*, *61*, 68–80. https://doi.org/10.1016/j.jog.2012.07.007

Schuh, H., & Böhm, J. (2013). Very Long Baseline Interferometry for Geodesy and Astrometry. In G. Xu (Hrsg.), *Sciences of Geodesy—II* (S. 339–376). Springer Berlin Heidelberg. https://doi.org/10.1007/978-3-642-28000-9_7

Böhm, J., Böhm, S., Boisits, J., Girdiuk, A., Gruber, J., Hellerschmied, A., Krásná, H., Landskron, D., Madzak, M., Mayer, D., McCallum, J., McCallum, L., Schartner, M., & Teke, K. (2018). Vienna VLBI and Satellite Software (VieVS) for Geodesy and Astrometry. *Publications of the Astronomical Society of the Pacific*, *130*(986), 044503. https://doi.org/10.1088/1538-3873/aaa22b

Böhm, J., & Schuh, H. (Hrsg.). (2013). *Atmospheric Effects in Space Geodesy*. Springer Berlin Heidelberg. https://doi.org/10.1007/978-3-642-36932-2

Nothnagel, A. (2023). Elements of Geodetic and Astrometric Very Long Baseline Interferometry.

Whitney, A. R., Rogers, A. E. E., Hinteregger, H. F., Knight, C. A., Lippincott, S., Levine, J. I., Clark, T. A., Shapiro, I. I., Robertson, D. S. (1976) A very-long-baseline interferometer system for geodetic applications. Radio Science 11(5), pp. 421-432

Navratil, G. (2020). Ausgleichungsrechnung Vertiefung

Kupiszewski, P., Grinde, G., Garcia-Espada, S., Bolano Gonzales, R., (2020). Ny-Alesund Geodetic Observatory (IVS Report).

James, G. et al. (2023). An Introduction to Statistical Learning, Springer Texts in Statistics, https://doi.org/10.1007/978-3-031-38747-0_3

Lambert, S. et.al., (2006). A comparison of R1 and R4 IVS Networks (IVS Report).

Thomas, C. et.al., (2018). Performance of the Operational IVS-R1 and IVS-R4 Sessions.

Böhm, J. (2021). *Modern Space Geodetic Techniques (lectures WS21/22)*.

External links:

Blewitt et.al., (2018). http://geodesy.unr.edu/NGLStationPages/stations/NYA1

www.cmr.earthdt.nasa.goverment – NASA EARTH DATA (Open access for open science).

https://ggos.org/item/ivs/ - Global Geodetic Observing System (GGOS).

https://www.iers.org – International Earth Rotation and Reference System Service

https://vievswiki.geo.tuwien.ac.at/VLBI-Analysis - VieVS Wiki.

https://www.craf.eu/radio-observatories-in-europe/ny-alesund - Committee on Radio Astronomy Frequencies CRAF.

https://www.iers.org/IERS/EN/DataProducts/ITRS/itrs.html - The Interational Terrestrial Refrence System (ITRS).
https://ivscc.gsfc.nasa.gov – International VLBI Service for Geodesy & Astrometry.

http://geodesy.unr.edu/NGLStationPages/GlobalStationList - Nevada Geodetic Laboratory.

https://earth.gsfc.nasa.gov/geo/instruments/vlbi-global-observing-system-vgos. NASA Earth Sciences – VLBI Global Observing System (VGOS).

https://cddis.nasa.gov/Data_and_Derived_Products/VLBI/vlbi_l2_vgosDB_001.html. NASA Earth Data – CDDIS VLBI level 2 vgosDB format data (doi.org/10.5067/VLBI/VLBI_L2_VGOSDB_001).

https://transformator.bev.gv.at/at.gv.bev.transformator - Federal Office of Metrology and Surveying.

https://itrf.ign.fr – ITRF Website.

https://home.engineering.iastate.edu/~shermanp/AERE432/lectures/Rate%20Gyros/Allan%20variance.pdf – Allan Variance